



MSU Graduate Theses

Summer 2017


Study of Nano-Bio Interfaces in Nano-Bio Conjugates: Nanoparticles of Zinc Oxide (ZnO) and Biomolecules of Glucose, Cytosine, and Thymine

Bithi Paul

Missouri State University, Bithi2015@live.missouristate.edu

As with any intellectual project, the content and views expressed in this thesis may be considered objectionable by some readers. However, this student-scholar's work has been judged to have academic value by the student's thesis committee members trained in the discipline. The content and views expressed in this thesis are those of the student-scholar and are not endorsed by Missouri State University, its Graduate College, or its employees.

Follow this and additional works at: <https://bearworks.missouristate.edu/theses>

 Part of the [Biological and Chemical Physics Commons](#), [Biology and Biomimetic Materials Commons](#), [Semiconductor and Optical Materials Commons](#), and the [Structural Materials Commons](#)

Recommended Citation

Paul, Bithi, "Study of Nano-Bio Interfaces in Nano-Bio Conjugates: Nanoparticles of Zinc Oxide (ZnO) and Biomolecules of Glucose, Cytosine, and Thymine" (2017). *MSU Graduate Theses*. 3252.
<https://bearworks.missouristate.edu/theses/3252>

This article or document was made available through BearWorks, the institutional repository of Missouri State University. The work contained in it may be protected by copyright and require permission of the copyright holder for reuse or redistribution.

For more information, please contact bearworks@missouristate.edu.

**STUDY OF NANO-BIO INTERFACES IN NANO-BIO CONJUGATES:
NANOPARTICLES OF ZINC OXIDE (ZnO) AND BIOMOLECULES OF
GLUCOSE, CYTOSINE, AND THYMINE**

A Masters Thesis

Presented to

The Graduate College of

Missouri State University

In Partial Fulfillment

Of the Requirements for the Degree

Master of Science, Materials Science

By

Bithi Paul

August 2017

Copyright 2017 by Bithi Paul

**STUDY OF NANO-BIO INTERFACES IN NANO-BIO CONJUGATES:
NANOPARTICLES OF ZINC OXIDE (ZnO) AND BIOMOLECULES OF
GLUCOSE, CYTOSINE, AND THYMINE**

Physics, Astronomy, and Materials Science

Missouri State University, August 2017

Master of Science

Bithi Paul

ABSTRACT

Nano conjugates, composites of inorganic nanomaterials and bio molecules such as DNA, RNA and proteins, establish a sequence of wide varieties of nano-bio boundaries. The formation of these boundaries strongly depends on bio physicochemical reaction of biomolecules coated on the surface of nanomaterials. I am investigating various nano-bio conjugates consisting of zinc oxide (ZnO) nanoparticles with simple biomolecules including glucose and the nitrogenous bases of DNA such as cytosine and thymine. All nano-bio conjugates were fabricated using a standard bio-chemical synthesis process. Structural, physical, bio-chemical interface properties of nano-bio composites were probed using X-ray diffraction (XRD), Raman spectroscopy, and photoluminescence (PL) spectroscopy, X-ray photoelectron spectroscopy (XPS), scanning electron microscope (SEM). PL data indicate a visible green emission associated mainly with the oxygen vacancies on the surface of ZnO nanostructure. Oxygen vacancies have been modified with glucose bio molecules through capturing the free electrons on the surface layer. ZnO-DNA base Raman spectra indicate a strong cation (Zn^{2+}) affinity on $\text{C}_2=\text{O}_7$, $\text{N}_1\text{-H}$ or $\text{N}_3\text{-H}$ bonds. The inorganic-organic conjugates may be applied to elucidate the nano-bio interface more significantly, such as for targeted drug delivery, bioimaging, biomolecular sensing, and nanomedicine.

KEYWORDS: ZnO, glucose, thymine, cytosine, surface defect, photo luminescence

This abstract is approved as to form and content

Kartik Ghosh, PhD
Chairperson, Advisory Committee
Missouri State University

**STUDY OF NANO-BIO INTERFACES IN NANO-BIO CONJUGATES:
NANOPARTICLES OF ZINC OXIDE (ZnO) AND BIOMOLECULES OF
GLUCOSE, CYTOSINE, AND THYMINE**

By

Bithi Paul

A Masters Thesis
Submitted to the Graduate College
Of Missouri State University
In Partial Fulfillment of the Requirements
For the Degree Master of Science, Materials Science

August 2017

Approved:

Kartik Ghosh, PhD

Mahua Biswas, PhD

Adam Wanekaya, PhD

Julie Masterson, PhD: Dean, Graduate College

In the interest of academic freedom and the principle of free speech, approval of this thesis indicates the format is acceptable and meets the academic criteria for the discipline as determined by the faculty that constitute the thesis committee. The content and views expressed in this thesis are those of the student-scholar and are not endorsed by Missouri State University, its Graduate College, or its employees.

ACKNOWLEDGEMENTS

It is my great pleasure to having an opportunity to pursue my graduate research in the Physics, Astronomy, and Material Science department at Missouri State University. I would like to thank my thesis supervisor and mentor Dr. Kartik Ghosh for his continuous supports, precious suggestions, and guidance throughout my graduate study. I would like to thank to Dr. Biswas and Dr. Wanekeya for being valuable members of my thesis committee.

I am thankful to Dr. Mayanovic for helping me with several experimental techniques and Dr. Adam Wanekeya for allowing me to use the research facilities of Chemistry department and for being a board member of my thesis. I am grateful to Rishi Patel, JVIC for collecting high quality XPS data of my thesis. I would also like to thank Dr. Cornelison, Dr. Mitra, Dr. Mayanovic, and Dr. Sakidja for discussing science during my graduate tenure at MSU. I would like to thank all my colleagues for their inexorable support regarding this research work. Especially, I am thankful to Tamzid Ibn Minhaj for his critical reviews, which helped me do better research.

I am grateful to my parents and my younger siblings for their constant moral support to finish my graduate degree. I am also thankful to my spouse for inculcating in me the importance of higher studies and to achieving my professional goal. Without the help of all my dear and near ones the present research study would have been impossible.

TABLE OF CONTENTS

Chapter 1: Introduction	1
Chapter 2: Detection of glucose concentration through nano-bio interaction of glucose and ZnO nanoparticle.....	5
Abstract	5
Introduction.....	6
Experiment.....	9
Results and Discussion	10
Conclusions.....	23
References.....	24
Chapter 3: Probing the Interaction at the Nano-Bio Interface Using Optical and X-ray Spectroscopies: ZnO Nanoparticles, Cytosine and Thymine Biomolecules	26
Abstract	26
Introduction.....	27
Experiment.....	28
Results and Discussion	29
Conclusions.....	47
References.....	48
Chapter 4: Conclusions	51
Chapter 5: References	53

LIST OF TABLES

Table 2.1: Observed area for the different glucose concentration with ZnO nanoparticles	20
Table 2.2: Observed concentrations (atom %) of the elements by EDX	22
Table 3.1: Lattice parameters, c/a ratio of sample-A, D, and E.....	31
Table 3.2: Assignments of the vibrational mode of thymine, hydrolysis thymine and ZnO-thymine nanoconjugate	37
Table 3.3: Assignments of the vibrational modes of cytosine, hydrolyzed cytosine, and ZnO-cytosine nanoconjugates.....	40
Table 3.4: PL peak positions (nm) and the defect area (nm ²).....	43
Table 3.5: Zn and O concentrations (atom %) on ZnO and nanoconjugates	45

LIST OF FIGURES

Figure 2.1: XRD pattern of ZnO nanoparticles (a), XRD of PB-J nanoconjugate (b), and comparison of XRD pattern of four different nanoconjugates (c)	10
Figure 2.2: Raman spectrum of ZnO nanoparticles (a), Raman spectra of hydrolyzed glucose (b).....	12
Figure 2.3: Raman spectra of sample PB-J (a), and comparison of all samples (b)	14
Figure 2.4: PL spectra of ZnO Bulk (a), ZnO Nanoparticle (b)	15
Figure 2.5: Photoluminescence spectra of all samples with different glucose concentration in normal scale (a), and in log scale (b)	16
Figure 2.6: Decreasing of defect peak area after incorporation with glucose on ZnO nanoparticles	19
Figure 2.7: PL fitted data of sample PB-J.....	19
Figure 2.8: TEM images of ZnO nanoparticle in different scale	21
Figure 2.9: SEM images of ZnO nanoparticles (a), ZnO-glucose nanoconjugate (b)	21
Figure 2.10: XPS data of Zn 2p core level (a), and O 1s core level (b).....	22
Figure 3.1: XRD pattern of ZnO nanoparticles (a), sample-D (b), and sample-E (c)	30
Figure 3.2: Raman spectra of ZnO nanoparticle	32
Figure 3.3: Molecular structure of thymine	33
Figure 3.4: Molecular structure of cytosine	34
Figure 3.5: Raman spectra of thymine powder (a), and hydrolyzed thymine (b)	34
Figure 3.6: Comparison Raman spectra of thymine powder and hydrolyzed thymine (a), and Raman spectra of thymine powder, hydrolysis thymine, and sample-D (b).....	36
Figure 3.7: Raman spectra of cytosine powder (a), and hydrolysis cytosine (b).....	38
Figure 3.8: Comparison of Raman spectra of cytosine powder and hydrolyzed cytosine (a), comparative Raman spectra of sample-A, B, E (b), comparative Raman spectra of cytosine powder, sample-A, B, and E (c)	39

Figure 3.9: Room Temperature PL spectra of ZnO Bulk (a), and ZnO nanoparticle (b) ..	41
Figure 3.10: PL spectra of ZnO (Black), sample-D (Red), and sample-E (Blue).....	42
Figure 3.11: SEM images and EDX data of sample PB-D (Top), sample PB-E (Bottom)	44
Figure 3.12: TEM images of ZnO nanoparticle.....	44
Figure 3.13: XPS data of Zn 2p core shell level on ZnO, ZnO-cytosine nano-conjugate (a), ZnO, ZnO-thymine conjugate (b).....	45
Figure 3.14: X-ray photoelectron spectra of N 2p core shell electron of cytosine, ZnO-cytosine nano-bio conjugate (a) and thymine, ZnO-thymine nano-bio conjugate (b).....	46
Figure 3.15: XPS data of O 1s core shell (a), and C 1s core shell (b) of ZnO, thymine, and ZnO-thymine nano-bio conjugates	47

CHAPTER 1: INTRODUCTION

Nanotechnology has been developing fast with the tremendous advancements of biomedical applications for last few decays. To increase the development of nanotechnology, nanomaterials are being used exceedingly for the investigation of nano-bio applications. The unique structural and chemical properties of many nanomaterials are the main attractions to be used significantly for not only the device applications but also biological applications¹. Along with all other salient and effectual possessions, environmental friendly, biocompatible, biodegradable, and nontoxic nanomaterials have also accelerated the developments of nano-bio technology with great achievements.

Nanoparticles with tunable shape and size can provide unique optical, electrical, magnetic, and chemical properties, and those features are favorable for many biological applications. Due to having uniform shapes (eg; nano rod, nanotubes, and nanowires) and particle sizes, metal and semiconductor oxides can be used to study nano-bio interactions². Among all oxide semiconductors, zinc oxide (ZnO) is the best inorganic material for nano-bio interactions as it exhibits unique structural, chemical, optical, and electrical properties. ZnO has a wide band gap (3.37eV), a high excitation binding energy (60 meV), unique optical and piezoelectric properties, and all these properties allow ZnO to be investigated for device applications in nanotechnology^{1,3-9}.

Apart from the device applications, due to having low toxicity and easy fabrication method, ZnO nanoparticles are now being widely used for the development of biomedical applications¹. Zhang *et al.*² claimed that zinc ion (Zn^{+2}) is an indispensable bench-mark ion for human body to various aspects of metabolism. It is also suggested

that around 11 mg of Zn^{+2} is needed for adults per day in United States¹. In addition, ZnO is such a molecule which can be dissolved in both acidic as well as basic solutions, and the solubility in acidic solution can be compatible to use for tumor cells, tumor microenvironment¹. These noteworthy properties make ZnO nanoparticles as a well suited biocompatible nanomaterial for the biomedicine investigation.

Deoxyribose nucleic acid (DNA), ribose nucleic acid (RNA), and glucose are fundamental units for all living organism. DNA and RNA are generally constructed as a long polymer with ribose sugar and phosphate backbone, and both play an important role in carrying genetic information. Glucose is considered as a vital energy source which circulates throughout the body by blood circulation. Though glucose is important for human body, excessive glucose in blood causes diabetes. It is reported that about 200 million people are affected by diabetes in the world and diabetes is becoming a principle causes for many fetal diseases like kidney failure, heart disease, blindness, even death¹⁰. So, it is now highly concerned matter to expansion of reliable glucose sensor with magnificent sensitivity in medical since as well as food industries¹⁰⁻¹². In recent days, the developments of photonics technology create the tremendous opportunity to investigate several optical methods for sensing diabetes¹³.

DNA and RNA polymers consist of four nitrogenous bases, three bases are common for both namely adenine, guanine, cytosine. Fourth base of the DNA is thymine, and thymine replaces by uracil for RNA. Since DNA, RNA, and glucose are the most important basic biological components for all living organism, it is extremely important to understand the molecular mechanism of these biomolecules for the development of modern life science researches. The nano-bio interaction between ZnO and simple

biological elements such; DNA, RNA, and proteins are now widely investigated for the developments of advanced nano-bio technology.

Nano-bio conjugates, composites of inorganic nanomaterials and organic biomaterials like proteins, nucleic acids, carbohydrates, establish a sequence of a wide varieties of nano-bio boundaries¹⁴. Engineering the interface of nano-bio composites is strongly relied on the chemical reactions between inorganic nanomaterials and organic bio materials. The nanobio conjugates are now utilized for electrochemical biosensors, targeted drug delivery, bioimaging, and nano medicine applications. The conjugates can be constructed with semiconductor oxide nanomaterials and simple organic biomolecules for the implements of biosensor. The nanomaterial based biosensors are engineered in such a way where a nanobio-interafce is designed with biologically active materials along with inorganic crystalline electrically and optically active nanomaterials¹⁵. ZnO provides both optical and electrical properties and it can translate the biological signals to the electronic signals which is useful to design a successful biosensor¹⁵. Not only for optical and electrical properties, ZnO is also considered as a biocompatible molecule to be investigated for nano-bio conjugates.

Here, I explored a new method to create nano-bio conjugates by using ZnO nanoparticles with basic biomolecules such as glucose and two basic nitrogenous units of DNA: thymine and cytosine and investigated nano-bio interfaces using various spectroscopic techniques. Results have been discussed in two papers. Paper-1 investigates the nano bio-conjugates of ZnO-glucose, and paper-2 investigates the ZnO-thymine, ZnO-cytosine composites. Both papers discuss the interfaces of conjugates to establish the importance of nano-bio composite materials for enlargement or evolution of nano-bio

technology. All nano-bio composites were fabricated by standard physicochemical method. The structural, physical, and physicochemical properties of nano-bio composites were probed by the Raman spectroscopy, X-ray diffraction spectroscopy (XRD), photoluminescence (PL) spectroscopy, scanning electron microscope (SEM), electron X-ray dispersion (EDX), transmission electron microscopy (TEM), and X-ray photoelectron spectroscopy (XPS).

CHAPTER 2: DETECTION OF GLUCOSE CONCENTRATION THROUGH NANO-BIO INTERACTION OF GLUCOSE AND ZNO NANOPARTICLE

Abstract

Nowadays, nano-bio interaction is the subject of intense research for many advanced biomedical applications. Zinc oxide (ZnO) is a well-studied oxide nanomaterial with several novel properties. Glucose is a simple biomolecule which circulates throughout the blood, and it is considered as a vital energy source for our muscles and tissues. In this paper, I have studied the binding of glucose concentration on the surface of ZnO nanoparticle using PL spectroscopy. All nano-bio composites were fabricated by using a standard bio-chemical synthesis method. Structural properties of the glucose, ZnO, and their interface were probed using X-ray diffraction (XRD), scanning electron microscopy (SEM), energy dispersive X-ray (EDX), photoluminescence spectroscopy (PL), X-ray photoelectron spectroscopy (XPS), and Raman spectroscopy techniques. Shifting “as well as,” relative intensity in peak position of some vibrational modes of glucose as well as ZnO in Raman spectra are clear indication of binding between glucose and ZnO nanoparticles. XPS and EDX data also support the Raman data. A visible green emission from ZnO particles is appeared in the PL data which is associated with the surface defects such as oxygen (O) vacancies, zinc (Zn) vacancies, Zn interstitials, oxygen antisites on the surface of ZnO nanostructure. Strong binding of glucose biomolecule on the surface of ZnO nanostructures, the green-yellow-orange emission are reduced by capturing the free electrons from the surface layer of ZnO nanostructure.

Surface binding study of ZnO nanoparticles with glucose using PL spectroscopy can be used for future application to glucose sensing.

Key words: zinc oxide, glucose, photoluminescence, surface area, defect peak, oxygen vacancy, vibration mode.

Introduction

“Over a few decades” nano-bio interaction has accelerated the developments of nano and bio technology. To being used for nano-bio interactions, nanomaterials of transition metal oxide are well suited for their unique properties like photoconductivity, electro conductivity, ferromagnetism, and piezoelectricity. Due to having these novel properties, nanoparticles of metal oxides such as ZnO, TiO₂, and Fe₃O₄ are now vastly useful in biosensors and nano-medicine.

ZnO is a well-known n type semiconductor having wide band gap (~3.37 eV) along with large excitation binding energy (~60meV) as well as excellent photoluminescence properties¹⁻⁸. Currently, ZnO nanostructures have great attention for extensive research due to their unique electrical and optical properties which allow this material to be used for diverse applications such as light emitting diode, piezo electric transducer, photovoltaics, transparent electrodes, gas sensors, bio imaging probes, light emitters, photo catalysis, and drug delivery⁹⁻¹⁰. Recently, it has become an attractive candidate for optical and optoelectronic applications due to its wide direct bandgap along with large excitation binding energy¹¹. Predominantly, ZnO nanostructure shows a near band-edge ultraviolet emission (around 385nm) and a broad defect visible green

emission (510-590 nm) on its photoluminescence spectrum. The defect peak is centered at around 2.3 electro volt (2.3eV) in bulk sample, whereas it is in around 2.4 eV for ZnO thin film¹⁰. The ultraviolet emission near the band edge is associated for the recombination of electron and hole from conduction band to the valance band and a broad visible green luminescence originated to the defect on surface¹. The visible luminescence is appeared in the yellow-orange range and in the green region due to the defect on ZnO surface layer¹⁰. Though the root of the strong green emission is still controversial the surface defect on the ZnO is mostly assigned for oxygen vacancies, oxygen antisites, interstitial oxygen, Zn vacancies, Zn interstitial, and dislocations¹. Among all of these possible reasons, oxygen vacancies and Zn interstitials are highly responsible for the broad luminescence peak to the defect level¹². Apart from these, defect also depends on the surface to volume ratio of nanoparticles, synthesis methods, particle size, and the impurity concentrations on the surface region⁹.

Single ionized oxygen vacancies on the surface of ZnO nanoparticles are mostly responsible for the defect peak in PL spectra that could also be correlated to the particle size and structural morphology. The intensity and width of green emission defect peak depend on the doping or the concentration of other impurities on the surface ZnO nanostructures¹⁰. Overall, the green visible emission is associated for nothing but the recombination of a shallow trapped electron with a hole in a deep trap and the recombination of an electron in singly ionized oxygen vacancies with a photo generated hole in the valence band^{9-10,13}. In addition, small sized nanoparticles contain depletion layer near the surface and the thickness of this layer depends on the density of native

carrier concentration which make the surface positively charged and ZnO end-up as n type semiconductor.

With the overgrowing developments of nanotechnology, nanomaterials are widely used for the enlargements of biotechnology by using the unique optical and electrical properties. Nanomaterials which can translate the biological signal throughout the electrical and optical signals have been probed for the nano-bio interactions. The interaction of nanomaterials with simple biomolecules can be used to create worthwhile nano-bio composites and the composites can be investigated for the diverse biological executions such as drug delivery, bioimaging, nanomedicine. Nano-bio composites, consisting of simple biomolecules (DNA, RNA, protein, and glucose) initiate a succession of nano-bio boundaries with strong chemical reactions. Glucose is one of the most important energy source of human body, and it circulates throughout the blood circulation. Monitoring the glucose on blood is one of the most vital sensing technology in clinical diagnostic as well as food industries¹⁴. For the last few decades, nanomaterials have been widely investigated for the biosensor applications with their unique structural, chemical and optical properties¹⁵. Along with unique optical properties, ZnO is a biocompatible, nontoxic nanomaterial which is also one of the most promising candidate to be used for biosensor applications. Zinc ion (Zn^{2+}) is an important element for human body and it is also suggested that around 11mg of Zn^{2+} is needed for an adult per day in United States⁸.

In this study, a noble method has been probed to create nano-bio composite with ZnO nanoparticles and basic biomolecule glucose. Structural properties of the glucose, ZnO, and their interface were probed using X-ray diffraction, scanning electron

microscopy, energy dispersive X-ray, X-ray photoelectron spectroscopy, and Raman spectroscopy techniques. The composite has been investigated to modify the surface defects of ZnO nanostructures by using photoluminescence spectra. Different glucose concentrations have been used to modify the surface defect of nanostructures.

Experiment

D-alpha glucose and ZnO nanoparticles were purchased from Sigma Aldrich. The details of experimental synthesis of nano-bioconjugates are as follows: 0M, 0.055M, 0.112M, 0.167M, 0.223M, 0.444M, 0.555M concentrations of D-alpha glucose were added to the 20 mg of ZnO nanoparticles separately and kept the solutions for 2 hours in a desiccator at room temperature. After then solutions were centrifuged (LW Scientific centrifuge, Model D8) at a rotation speed of 30 revolutions per second for 20 minutes. The precipitations were dried at room temperature. Per the glucose concentrations (above mentioned) with 20 mg ZnO nanoparticles, samples were given the names as: STD, PB-A, PB-B, PB-C, PB-D, PB-F, PB-H, and PB-J respectively. The powder diffraction patterns of the prepared samples were investigated by X-ray diffraction (XRD; Bruker; D8; θ -2 θ scan with Cu K α ($\lambda=1.5405 \text{ \AA}$)). The average particle sizes also calculated from the XRD data using Debye-Scherrer formula, $d=0.89\lambda/\beta\cos\theta$ where λ is the x-ray wavelength, θ is Bragg's diffraction angle and β is the peak width at half maximum. The morphology and elemental analysis of as-prepared samples were carried out by scanning electron microscopy (SEM; FEI Quanta 200S) and electron dispersive spectroscopy (EDS). The vibrational phonon modes were determined by employing micro Raman Spectroscopy using 532 nm green laser (Horiba Labram Raman-PL) and

Photoluminescence measurements were investigated using 325 nm UV laser by the above-mentioned instruments. The PL spectra were analyzed using Gaussian peak fittings by OriginPro 8.5.1 software. XPS was used to analyze the surface structure of nano-bio conjugates.

Results and Discussion

To investigate the crystal structure properties of ZnO nanoparticles and the ZnO-glucose nanoconjugates, XRD data were collected very carefully. Figures 2.1(a-c) show the XRD pattern of pure ZnO nanoparticles and ZnO-glucose nano-bio conjugates. The observed, calculated (by Rietveld refinement), and different XRD patterns are shown by black, red, and blue colors respectively. All samples were placed per the Bragg-Brentano reflection geometry during XRD experiment.

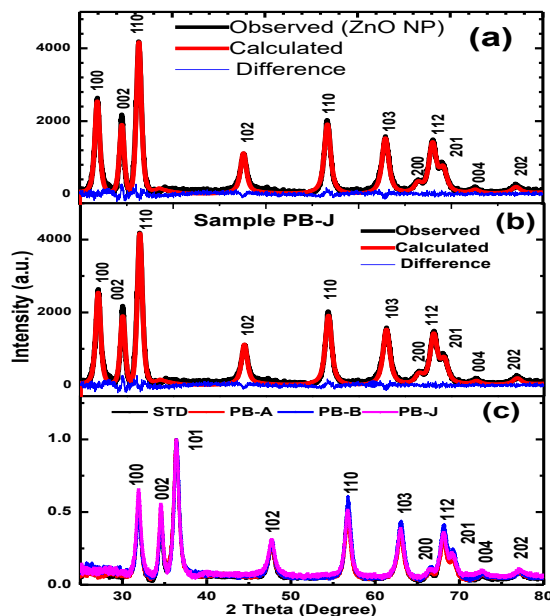


Figure 2.1: XRD pattern of ZnO nanoparticles (a), XRD of PB-J nanoconjugate (b), and comparison of XRD pattern of four different nanoconjugates (c)

Correct calibrations, all axis (X, Y, and Z) alignment of the samples, suitable data acquisition time were taken under consideration before collection of XRD data. To get the good refinement results, some parameters were taken under consideration (zero error, absorption correction factors). The calculated goodness of fit (GOF) from Rietveld refinement was close to 1 after appropriate corrections employing spherical harmonics. An order of 5 was used to Chebyshev background correction. XRD data for all samples confirm the crystal structure of ZnO nano powder and we did not find any change of zinc oxide crystal structure after interaction with different glucose concentrations. XRD data confirm the crystallographic structure of ZnO nanoparticles which indicates that ZnO nanoparticles of all samples are crystallized as *P63mc* (hexagonal close-packed crystal structure).

ZnO is a highly Raman active, and it has six significant vibrational phonon modes namely, A_1 , E_1 , E_2 , and B_1 . But B_1 phonon is not Raman active whereas rest of the modes are strongly visible in Raman spectra². The A mode indicates the molecular vibration along z-axis and both E_1 and E_2 are denoted for X-Y plane vibrations. Two significant sharp Raman peaks at 438cm^{-1} and 580cm^{-1} are associated for the $E_2(\text{high})$ and the $A_1(\text{LO})$ mode respectively¹⁰. Figure 2.2(a,b) show the Raman spectrum of ZnO nanoparticles and Raman spectra of hydrolyzed glucose using 532 nm wavelength green laser source. Figure 2.2(a) and Figure 2.2(b) probed the signature Raman vibrational modes of ZnO nanoparticles and glucose bio molecules respectively. The Raman spectrum of ZnO nanoparticles reveals two prominent peaks at 438cm^{-1} and 580cm^{-1} along with some weak features at around 336cm^{-1} , 500cm^{-1} , 984cm^{-1} , 1046cm^{-1} , and 1094cm^{-1} . The peak position at 336cm^{-1} appears due to the low frequency bands

associated with the difference between two modes $E_2(\text{High})$ and $E_2(\text{Low})$ and it is denoted as $E_{2H}-E_{2L}$ mode¹⁶. The sharpest Raman peak centered at 438cm^{-1} corresponds to the oxygen vibration in hexagonal crystalline along the X-Y plane, and this peak becomes wider with higher concentration of foreign molecule on ZnO surface area¹⁷.

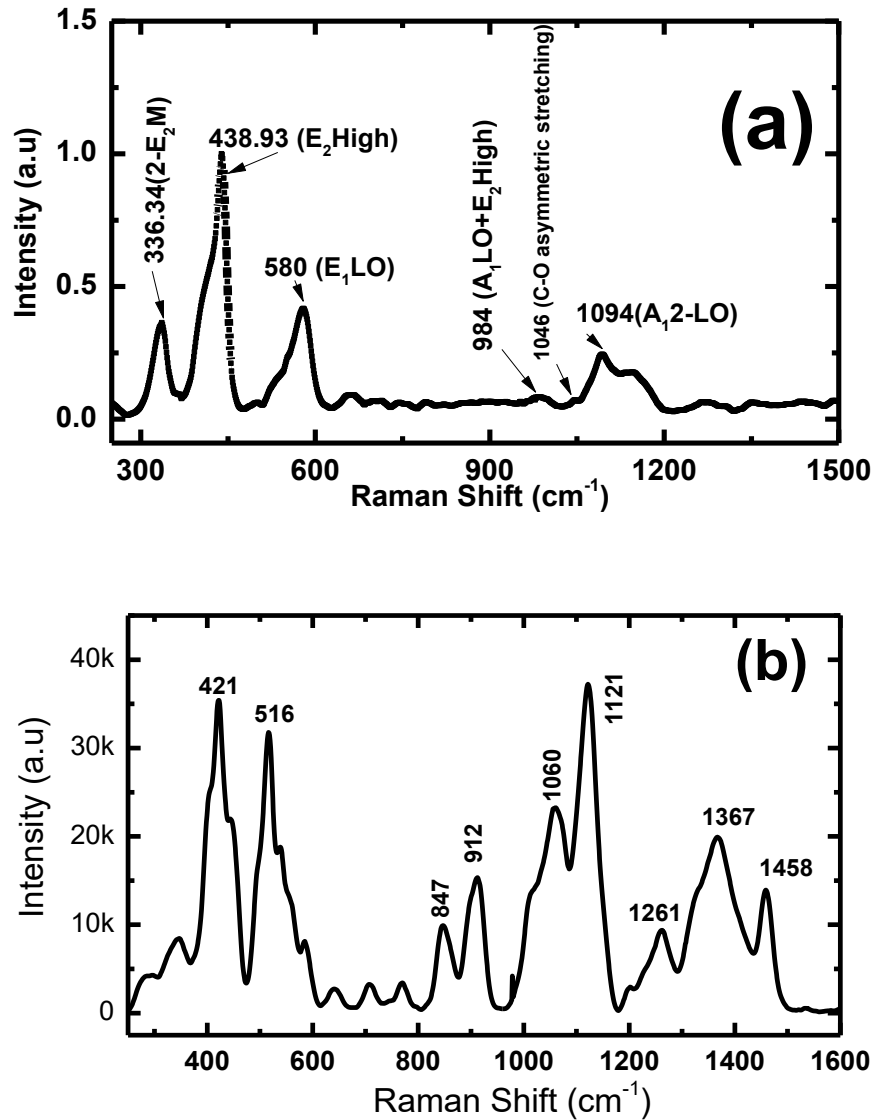


Figure 2.2: Raman spectrum of ZnO nanoparticles (a), Raman spectra of hydrolyzed glucose (b)

This peak belongs to $E_2(\text{High})$ mode and indicates the more homogenous distribution of grain size as well as dimensions of the nanoparticles². The intensity of this prominent sharp peak increases with the increase of particle size. In my all samples, 438 cm^{-1} appears as the most intense peak that revealed our samples more homogeneously distributed with significant particle size. The second sharp peak at 580 cm^{-1} is associated for E_1 longitudinal optical (LO) mode with oxygen deficiency in ZnO nanoparticles¹⁸. This mode is affected by the impurity and the defect of nanoparticles. The peak at 580 cm^{-1} appears due to the presence of oxygen vacancy as well as Zn interstitials and particle size cannot modify the intensity of this mode². Basically, $E_1(\text{LO})$ modes point out the defect or the impurity on the ZnO nanoparticles and strongly correlated to the surface defect on ZnO nano powder². The $A_1(\text{LO})+E_2$ High mode has been assigned for the corresponding peak at 984 cm^{-1} which is associated for the vibration of two phonon combination². Another peak at 1094 cm^{-1} was found for the secondary A_1 longitudinal optical (2LO) mode which is associated for the molecular vibration along the z-axis. A very weak peak at 1046 cm^{-1} is associated for the C-O asymmetric mode of carboxylate defect group, and this peak is affected by the surface area and the particle size¹⁷. The intensity of this peak is increased with the increase of particle size. Another weak signal at 500 cm^{-1} is associated, but the explanation of this peak is rarely found from the literature. It may appear for the oxygen vacancies of defect area of ZnO nanopowder.

Figure 2.3(a) shows the Raman spectra of sample PB-J having 0.555M glucose concentration with ZnO nanoparticles by using 532 nm green laser source. Figure 2.3(b) shows the comparison of Raman spectra for different glucose concentrations on ZnO nanoparticles. From the literature, eight active Raman modes of glucose are found at

around 436 cm^{-1} , 526 cm^{-1} , 855 cm^{-1} , 912 cm^{-1} , 1065 cm^{-1} , 1126 cm^{-1} , 1365 cm^{-1} , and 1456 cm^{-1} ¹⁹. Figure 2.3(a) confirms the finger print of hydrolyzed glucose at around 438 cm^{-1} , 522 cm^{-1} , 544 cm^{-1} , 853 cm^{-1} , 912 cm^{-1} , 1127 cm^{-1} , and 1371 cm^{-1} .

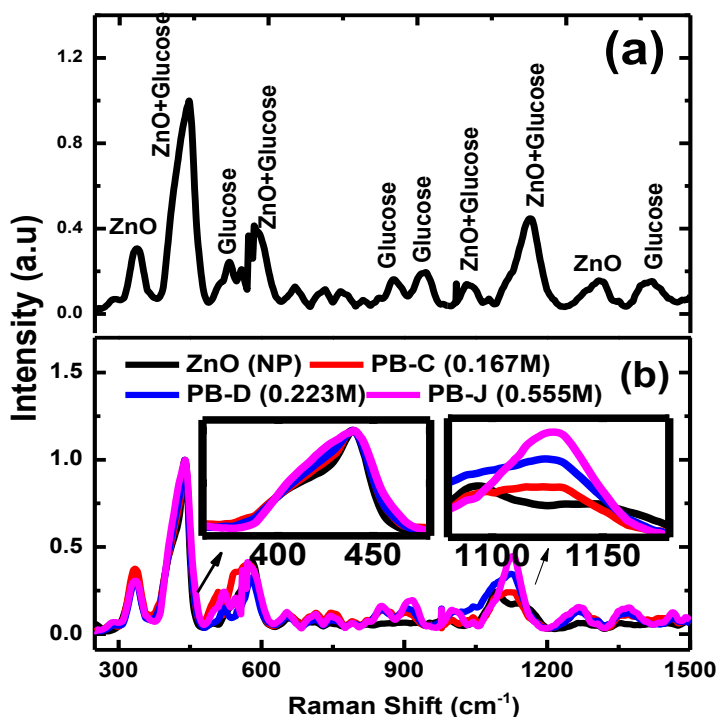


Figure 2.3: Raman spectra of sample PB-J (a), and comparison of all samples (b)

Comparing the Raman data of standard ZnO nanoparticles and ZnO-glucose nanocomposite (sample PB-J), one can see that the peak at 438 cm^{-1} is becoming wider with the higher concentration of glucose. Figure 2.3(b) also indicates that with the higher concentration of glucose the E_2 (High) mode of ZnO nanoparticles is becoming wider. It concludes that after the interaction of ZnO with glucose the particle size is increasing with the higher concentration. Another significant peak at 1127 cm^{-1} which appears due to glucose concentration. This peak proved the presence of glucose on ZnO nanoparticles

and the intensity of this peak is increased with the increase of glucose concentration¹⁹. Glucose concentration of human body can be also detected by the intensity of this peak. The peaks at around 852cm^{-1} and 912 cm^{-1} are the signature finger print of glucose, and these peaks are not there at the ZnO nanoparticles. Thus, from the analysis of optical vibrational Raman modes, glucose concentration can be identified successfully.

Figures 2.4(a,b) show the photoluminescence (PL) spectra of ZnO bulk and ZnO nanoparticles, respectively. All PL spectra were collected at room temperature using Raman-PL spectrometer (Horiba Labram Raman-PL) using 325 nm laser source.

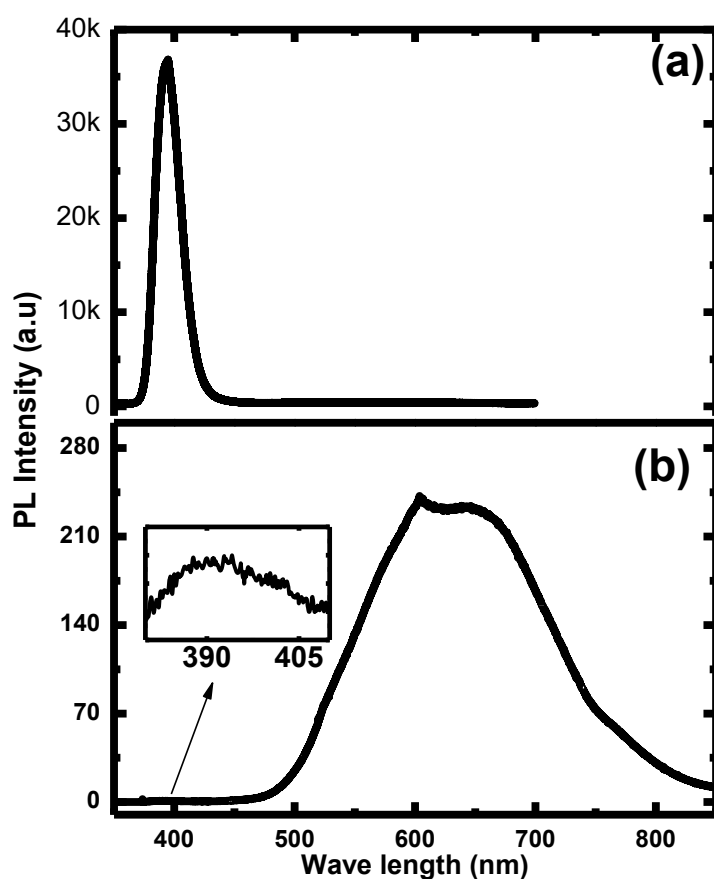


Figure 2.4: PL spectra of ZnO Bulk (a), ZnO Nanoparticle (b)

ZnO bulk particles don't show any green emission whereas nanoparticles reveal a wide green emission peak. Figure 2.5(a,b) indicate the PL spectra of all samples in different intensity scales at room temperature. All spectra show an excitation peak at around near the bandgap (390nm) and a broad visible green luminescence from 1.7eV – 2.7eV having the maximum intensity at around 2.02eV.

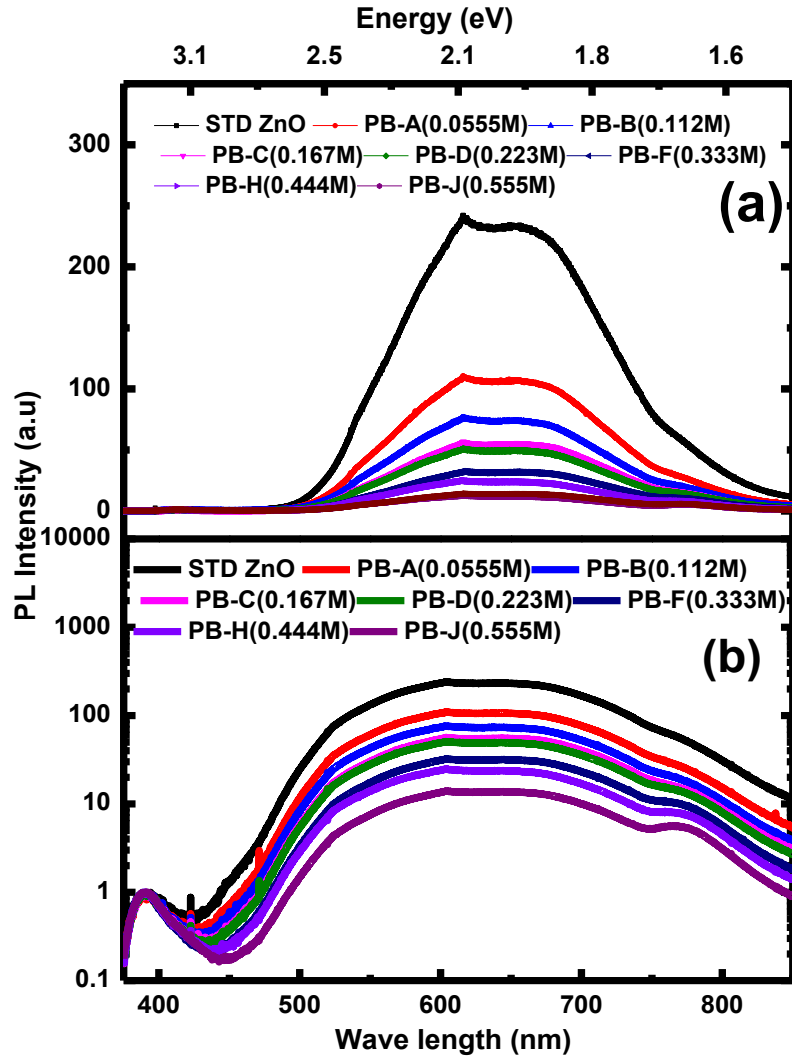


Figure 2.5: Photoluminescence spectra of all samples with different glucose concentration in normal scale (a), and in log scale (b)

In the PL spectra of all samples, it is clearly noticeable that the intensity of green emission is significantly higher than the intensity of blue emission near the bandgap and green emission decreases with the increase of glucose concentration. I normalized the intensity of blue emission (near the bandgap) for all samples to make easy comparison of green emissions for various glucose concentrations.

PL spectra of all samples is dominated by the defect peak (green emission) which is originated due to surface defects of nanoparticles. The green emission is considered for oxygen vacancies, Zn interstitials, oxygen antisites, and Zn vacancies¹⁰. With the increase of glucose concentration, the green emission decreases. From the PL data, it can be claimed that the surface area of ZnO nanoparticles is modified with the embodiment of glucose biomolecule, and higher the concentration, higher the reduction of green emission. Green emission depends on the particle size, synthesis method, oxygen vacancies, and the ratio of surface area to volume¹. The data implied that the surface layers of ZnO nanostructures could be modified with the reduction of density of oxygen vacancies and the intensity and surface area of defect peak are decreasing with the increasing of glucose concentration. It can be determined that the particles on the surface layer of ZnO nanostructures are taking part of strong interaction with glucose biomolecules by absorbing the oxygen.

The spherical ZnO nanoparticles “which are on surface area” are taking part to quench the green emission mostly due to the removal of oxygen vacancy on the surface. Since all samples are prepared with double ionized (DI) water (18 M-Ohm) and glucose molecules with zinc oxide nanoparticles, it is possible that glucose ($C_6H_{12}O_6$) releases the hydrogen atom (H) and creates an anionic head group which then coordinating to Zn^{+2} for

filling the oxygen vacancies on or near the surface. Furthermore, oxygen is more negative in O-H and O-C bond, it tends to fill in oxygen vacancies. Hence, one can effectively reduce the density of oxygen vacancies near the surface area through introducing glucose on zinc oxide nanoparticles.

Since oxygen vacancies are considered for the main reason behind the surface defect or green emission on ZnO nanoparticles, the reduction of oxygen vacancies can suppress the green emission. On the surface, three types of oxygen vacancies are possible for three different charge states namely neutral oxygen vacancies (V_o^0), the singly ionized oxygen vacancies (V), and the double ionized oxygen vacancies (v)¹. When laser is being exposed to the sample electron-hole pairs are generated, quasi Fermi levels of hole and electron are shifted towards the valence band and conduction band respectively and the position of these fermi levels are determined by the density of photo generated carriers¹. Due to having the small volume of nanoparticles the fermi level of electron can be shifted with relatively lower excitation then the surface area will be accommodated with neutral vacancies finally, by the recombination of photo generated holes single ionized vacancies are formed¹. In addition, as double ionized vacancies are more stable than single ionized vacancies, double ionized vacancies are formed to lower the total energy.

Hence, the reduction of density of oxygen vacancies quenches the intensity as well as the area of green emission. Figure 2.6 shows the defect peak area of all samples in log scale. Figure 2.7 indicates the PL fitted data of sample PB-J. The PL data of all samples were fitted using OriginPro 8.5.1 software. Table 2.1 shows the surface area of defect peak with different glucose concentrations on ZnO nanoparticles and the defect peak area is decreased for higher glucose concentrations.

The area of defect peaks has been also calculated using OriginPro 8.5.1 software.

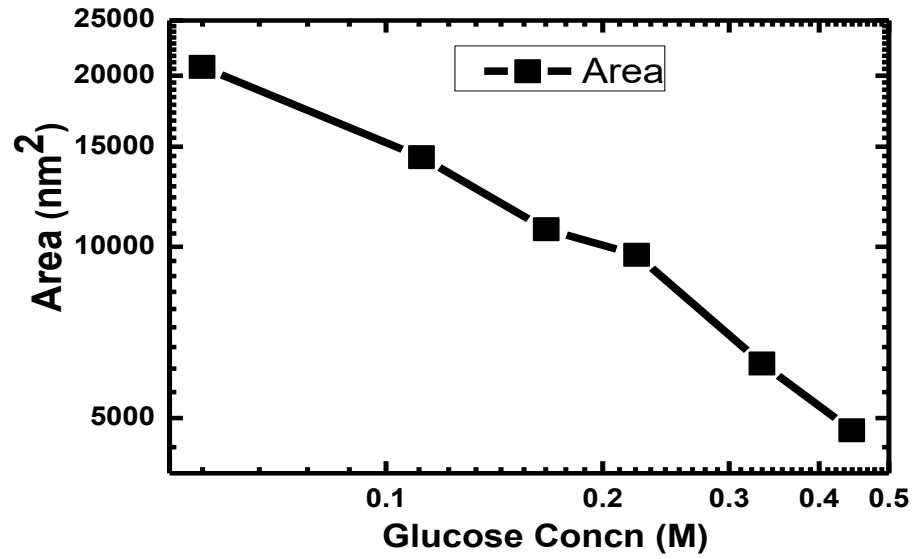


Figure 2.6: Decreasing of defect peak area after incorporation with glucose on ZnO nanoparticles

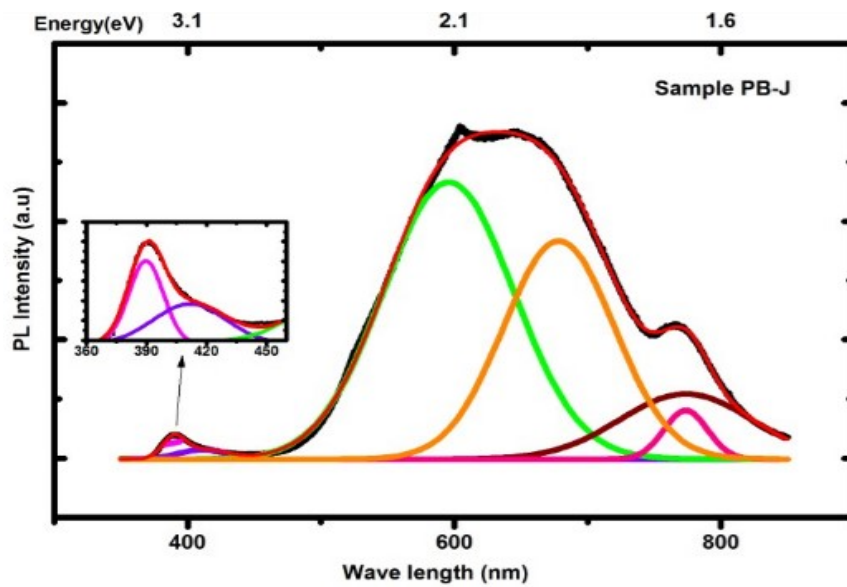


Figure 2.7: PL fitted data of sample PB-J

Table 2.1: Observed area for the different glucose concentration with ZnO nanoparticles

Sample ID	Glucose concentration (M)	Area (nm ²)
ZnO NP	0.000	45017
PB-A	0.055	20712
PB-B	0.112	14378
PB-C	0.167	10739
PB-D	0.022	9683
PB-F	0.333	6235
PB-H	0.444	4758
PB-J	0.555	2479

Figures 2.8 shows the transmission electron microscopy (TEM) images of ZnO nanoparticles in different scales. Figure 2.9(a,b) indicates SEM images of ZnO nanoparticles and nanoconjugates. Particle size of ZnO nanoparticle is found about 20-30 nm by using TEM data. The nature of nanoparticle was also confirmed using PL data which are discussed in previous section. SEM images reveal that there are no any significant changes of the morphology for ZnO nanoparticles and the nanoconjugate of ZnO with glucose.

EDX data confirm the different concentrations (atom %) of Zn and O for ZnO NP and sample PB-J. ZnO surface layer has oxygen vacancies so that after incorporation of glucose on ZnO, the oxygen atoms may be absorbed by the surface layer of nanostructure. Consequently, atomic percentage of oxygen atom has been increased for

ZnO-glucose nanoconjugate. Table 2.2 shows the atomic percentages of the elements of ZnO nanoparticles and nanoconjugate.

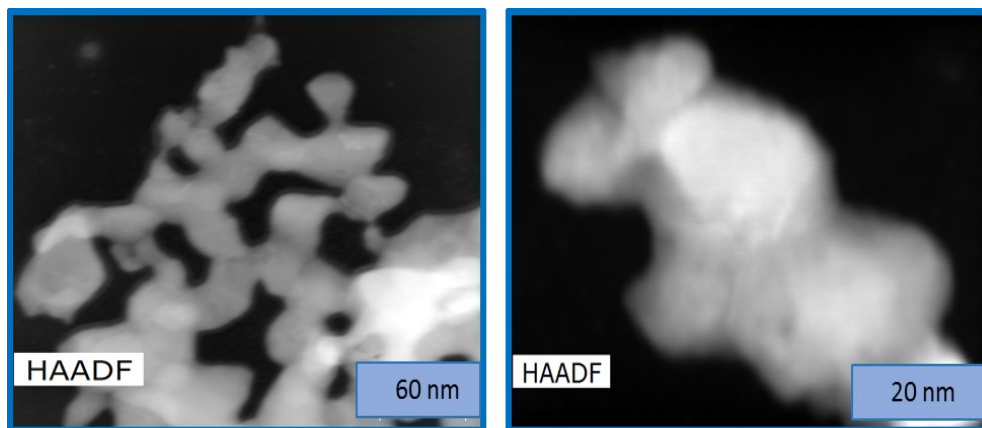


Figure 2.8: TEM images of ZnO nanoparticle in different scale

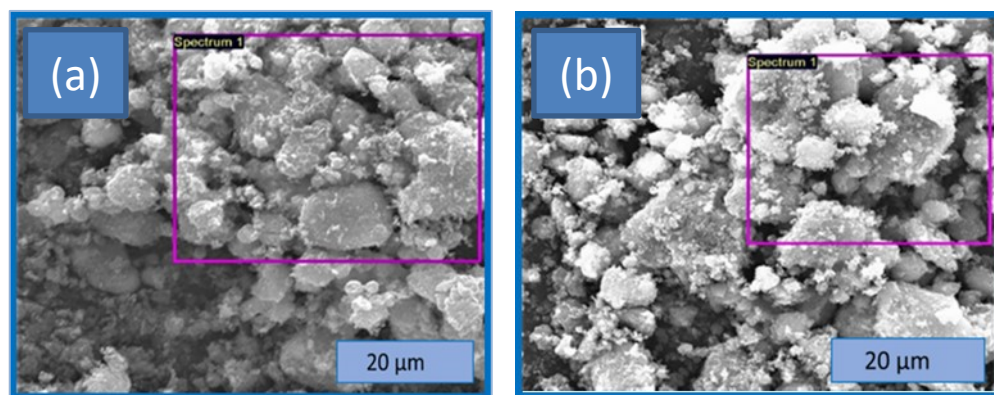


Figure 2.9: SEM images of ZnO nanoparticles (a), ZnO-glucose nanoconjugate (b)

Figures 2.10(a,b) indicate the XPS data of ZnO and ZnO-glucose nano-bio conjugates. Figure 2.10(a) represents the X-ray photoelectron spectra of the Zn 2p core

level of ZnO nanoparticles (black line), 0.055M glucose concentration of nano-bio conjugate (red line), and 0.55M glucose concentration conjugate (blue line).

Table 2.2: Observed concentrations (atom %) of the elements by EDX

Sample	Zn Conc	O Conc
ZnO NP	62.0	38.0
PB-J (0.555M)	56.6	43.4

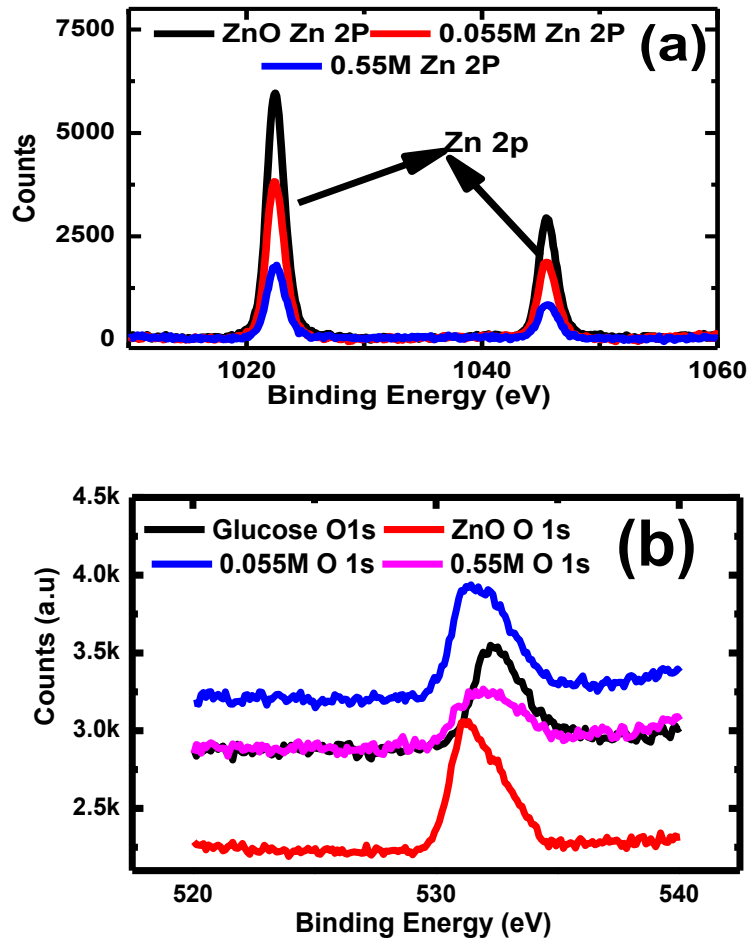


Figure 2.10: XPS data of Zn 2p core level (a), and O 1s core level (b)

Figure 2.10(b) shows the XPS of O 1s core level of ZnO nanoparticles and nano-bio conjugates with different glucose concentrations. XPS data reveal that the surface of ZnO nanoparticles is nicely coated with glucose biomolecules. The thickness of the coated layer is increased with the higher glucose concentration. Consequently, the intensity of Zn 2p peak is decreased. XPS data divulge that the binding energy of O 1s for ZnO and glucose biomolecules are different. The binding energy of O 1s core level for ZnO nanoparticle is around 531 eV whereas the binding energy is around 532 eV for the glucose biomolecules. The binding energy of O 1s core electron shell of the ZnO-glucose composite is in-between the binding energy of ZnO and glucose which were expected from our sample.

Conclusions

The main finding of this paper is that the surface defect of ZnO nanostructure is highly related to the oxygen vacancies and Zn_i which can be modified by absorbing oxygen from glucose biomolecule. The missing oxygen leaves the free electrons and increases the carrier density on ZnO nanostructure. Free electrons which are left from the oxygen vacancies are captured by absorbing the oxygen from glucose molecule. Consequently, the carrier density is decreased, and depletion width of the surface area is increased that may reduce the surface defect of ZnO nanostructure. Thus, the green emission which is originated by the oxygen vacancies can be reduced with the incorporation of glucose biomolecules. Hence, the study of ZnO-glucose nano-bio conjugate could be investigated for the diabetes sensor as well as improve the florescence property of ZnO nanoparticles which may be useful for bio imaging application.

References

1. Gong, Y., Andelman, T., Neumark, G. F., O'Brien, S. & Kuskovsky, I. L. Origin of defect-related green emission from ZnO nanoparticles: Effect of surface modification. *Nanoscale Res. Lett.* **2**, 297–302 (2007).
2. Wong, K. W. J. *et al.* Interaction of hydrogen with ZnO nanopowders—evidence of hydroxyl group formation. *Nanotechnology* **23**, 15705 (2012).
3. Srivastava, R. Investigation on Temperature Sensing of Nanostructured Zinc Oxide Synthesized via Oxalate Route. *J. Sens. Technol.* **2**, 8–12 (2012).
4. Demangeot, F. *et al.* Experimental study of LO phonons and excitons in ZnO nanoparticles produced by room-temperature organometallic synthesis. *Appl. Phys. Lett.* **88**, 71921 (2006).
5. Liu, J., Motta, N. & Lee, S. Ultraviolet photodetection of flexible ZnO nanowire sheets in polydimethylsiloxane polymer. *Beilstein J. Nanotechnol.* **3**, 353–359 (2012).
6. Alvi, N. ul H., Hussain, S., Jensen, J., Nur, O. & Willander, M. Influence of helium-ion bombardment on the optical properties of ZnO nanorods/p-GaN light-emitting diodes. *Nanoscale Res. Lett.* **6**, 628 (2011).
7. Kuriakose, S., Satpati, B. & Mohapatra, S. Enhanced photocatalytic activity of Co doped ZnO nanodisks and nanorods prepared by a facile wet chemical method. *Phys. Chem. Chem. Phys.* **16**, 12741 (2014).
8. Zhang, Y., Nayak, T. R., Hong, H. & Cai, W. Biomedical Applications of Zinc Oxide Nanomaterials. *Curr. Mol. Med.* **13**, 1633–1645 (2013).
9. Yadav, H. K., Sreenivas, K., Gupta, V., Singh, S. P. & Katiyar, R. S. Effect of surface defects on the visible emission from ZnO nanoparticles. *J. Mater. Res.* **22**, 2404–2409 (2007).
10. Camarda, P. *et al.* Luminescence mechanisms of defective ZnO nanoparticles. *Phys Chem Chem Phys* **18**, 16237–16244 (2016).
11. Singh, L. R. Photoluminescence Studies of ZnO, ZnO:Eu and ZnO:Eu Nanoparticles Covered with Y_2O_3 Matrix. *Mater. Sci. Appl.* **6**, 269–278 (2015).
12. Kumar, B., Gong, H., Chow, S. Y., Tripathy, S. & Hua, Y. Photoluminescence and multiphonon resonant Raman scattering in low-temperature grown ZnO nanostructures. *Appl. Phys. Lett.* **89**, 71922 (2006).

13. Zeng, H. *et al.* Blue Luminescence of ZnO Nanoparticles Based on Non-Equilibrium Processes: Defect Origins and Emission Controls. *Adv. Funct. Mater.* **20**, 561–572 (2010).
14. Yu, R., Pan, C., Chen, J., Zhu, G. & Wang, Z. L. Enhanced Performance of a ZnO Nanowire-Based Self-Powered Glucose Sensor by Piezotronic Effect. *Adv. Funct. Mater.* **23**, 5868–5874 (2013).
15. Zhuang, Z. *et al.* An improved sensitivity non-enzymatic glucose sensor based on a CuO nanowire modified Cu electrode. *The Analyst* **133**, 126–132 (2008).
16. Jan, T., Iqbal, J., Ismail, M. & Mahmood, A. Synthesis of highly efficient antibacterial agent Ag doped ZnO nanorods: Structural, Raman and optical properties. *J. Appl. Phys.* **115**, 154308 (2014).
17. Xiong, G., Pal, U. & Serrano, J. G. Correlations among size, defects, and photoluminescence in ZnO nanoparticles. *J. Appl. Phys.* **101**, 24317 (2007).
18. Rajalakshmi, M., Arora, A. K., Bendre, B. S. & Mahamuni, S. Optical phonon confinement in zinc oxide nanoparticles. *J. Appl. Phys.* **87**, 2445–2448 (2000).
19. Shao, J. *et al.* In Vivo Blood Glucose Quantification Using Raman Spectroscopy. *PLoS ONE* **7**, e48127 (2012).

CHAPTER 3: PROBING THE INTERACTION AT THE NANO-BIO INTERFACE USING OPTICAL AND X-RAY SPECTROSCOPIES: ZNO NANOPARTICLES, CYTOSINE AND THYMINE BIOMOLECULES

Abstract

Nano conjugates, composites of inorganic nanomaterials and biomolecules such as DNA, RNA and proteins, establish a sequence of wide varieties nano-bio boundaries. The formation of these boundaries strongly depends on bio physicochemical reactions of biomolecules with inorganic nanoparticles. It is very important to understand the nano-bio interfaces between nanomaterials and fundamental biomolecules such as glucose, RNA, DNA, ATP, and many others before using nano-bio conjugates in real life applications. Here, I report nano-bio interfaces consisting of zinc oxide (ZnO) nanoparticles with two nitrogenous bases cytosine and thymine of a DNA molecule. All nano-bio conjugates were fabricated using a standard bio-chemical synthesis process. Structural, physical, and interface properties of the nano-bio conjugates were probed using X-ray diffraction (XRD), Raman spectroscopy, photoluminescence (PL) spectroscopy, scanning electron microscopy (SEM), energy dispersive X-ray (EDX), and X-ray photoelectron spectroscopy (XPS). Experimental data indicates that ZnO nanostructures strongly interact with cytosine and thymine rings. Some vibrational modes in Raman spectra get modified with the incorporation of biomolecules. For example, Raman data of ZnO-thymine and cytosine composites indicate a strong zinc cation (Zn^{2+}) affinity of thymine and cytosine on C=O, N-H bonds. XPS and PL data also support the findings from Raman data. The inorganic-organic conjugates may be applied elegantly to

elucidate the nano-bio interface more significantly such as for targeted drug delivery, bioimaging, biomolecular sensing, and nanomedicine.

Keywords: nano-bio technology, nanomedicine, nano-bio conjugates, nano-bio interface, and Raman spectroscopy.

Introduction

Semiconducting oxides are now being widely used for their many novel properties to develop unique nano-bio conjugates, inorganic crystalline semiconducting materials which can translate the biological properties into electronic signals are the suitable candidates for nano-bio interactions¹. Among the list of semiconducting oxides, ZnO is the most widely used n type semiconductor having band gap along with large excitation binding energy. This material has diverse applications including light emitted diode, transparent electrodes, gas sensors²⁻¹⁰. Apart from the semiconducting device applications, ZnO nanoparticles has been used as drug delivery, cosmetics, bioimaging, nanomedicine due to its non-toxicity as well as bio compatibility phenomena². Easy fabrication of different nanostructures of ZnO; nanorod, nanotubes, nanowires, ZnO is another reason to select ZnO as a suitable candidate in making the nano-bio conjugates¹.

Nucleic acid is one of the most important bio components which can be used for the formation of nano-bio composites. Furthermore, DNA, a vital nucleic acid, plays important roles in genetic expressions as well as replications¹¹. DNA consists of four nitrogenous bases such as adenine, guanine, thymine, and cytosine which have individual significance to containing the genetic informations. Thus, it is very essential to study all

DNA bases to better understand the basic phenomena of nucleic acids and their mechanism to transferring the genetic signals. Among four bases of DNA, cytosine, and thymine are highly Raman active molecules so that nano-bio interfaces of ZnO-thymine and ZnO-cytosine composites can be probed by investigating the molecular vibrational modes. In presence of water molecules, thymine and cytosine both nitrogenous bases show the proton affinity on oxygen (O) and nitrogen (N) atoms due to the proton availability in water molecules¹¹⁻¹⁶. Not only the proton affinity, thymine and cytosine biomolecules exhibit the cation affinity with the incorporation of any ionic compound, and transition metal cations are highly favorable to the DNA bases among all metal cations¹⁴⁻¹⁵. It has been probed that N1-C2 and C2-N3 sites of thymine and cytosine are taken place to show the cation affinity by making the hydrogen bond with Zn^{2+} and proton (H^+)¹¹⁻¹².

Here, I report the complex formation of nano-bio conjugates consisting of inorganic ZnO nanostructures and two basic nitrogenous bases cytosine and thymine of a DNA molecule in presence of water molecule. To better understand the nano-bio interface of the nanoconjugates, physical, structural, and chemical properties were probed by the XRD, micro Raman spectroscopy, photoluminescence spectra, SEM, EDX, and XPS.

Experiment

Thymine, cytosine, and ZnO nanoparticles were purchased from Sigma Aldrich. The experimental synthesis details are as follows: 40 mg ZnO nanoparticles were added with 1 mL deionized water, 2 mg cytosine and 2 mg thymine were mixed with 1 mL

deionized water separately. All solutions were sonicated for 10 minutes to uniformly distribute the constituted solvent. The solution of cytosine, thymine and ZnO were separated into two 500 mL portions individually. Five mixtures of samples were prepared and are referred to as samples A, B, C, D and E. Sample A, B, and C contain only 500 mL of ZnO, 500 mL of cytosine and 500 mL of thymine, respectively. Sample D contains 500mL ZnO with 500mL thymine and sample E contains 500mL cytosine with 500mL ZnO. All samples were kept in a desiccator for 24 hours at room temperature. Then all samples were centrifuged (LW Scientific centrifuge, Model D8) at a rotation speed of 30 revolutions per second for 10 minutes to remove the loosely interacting constituents. The solid products were taken and dried in air for various characterizations. The powder diffraction data of all samples was taken by X-ray Diffraction (XRD; Bruker, D8 Discover). θ -2 θ scan was obtained by using Cu K α ($\lambda = 1.5405 \text{ \AA}$). Rietveld refinements of XRD data were carried out with Diffrac^{plus} Topas software. Raman and PL spectra were collected by Raman-PL system (Hariba Labram Raman-PL) using 532nm and 325 nm wave length laser source, respectively. The PL spectra were analyzed with Gaussian peak fittings by using OriginPro 8.5.1 software. The elemental analysis of the as-prepared samples was characterized by XPS and EDS and the morphology were determined by a SEM (SEM; FEI Quanta 200S).

Results and Discussion

XRD data of all samples were collected to know the structural properties of ZnO nanoparticles as well as nanoconjugates. Glass substrate has been used to prepare the sample for XRD experiment, and samples were placed per the Bragg-Brentano reflection

geometry during the experiment. Correct calibrations, all axis alignment of the samples, thickness of samples, geometry of the XRD instrument, and suitable data acquisition time were taken under consideration before collecting data.

Figures 3.1(a-c) show the XRD pattern of ZnO nanoparticles and nano-bio conjugates with thymine and cytosine. The observed, calculated by Rietveld refinement, and difference XRD patterns are shown by black, red, and blue colors respectively.

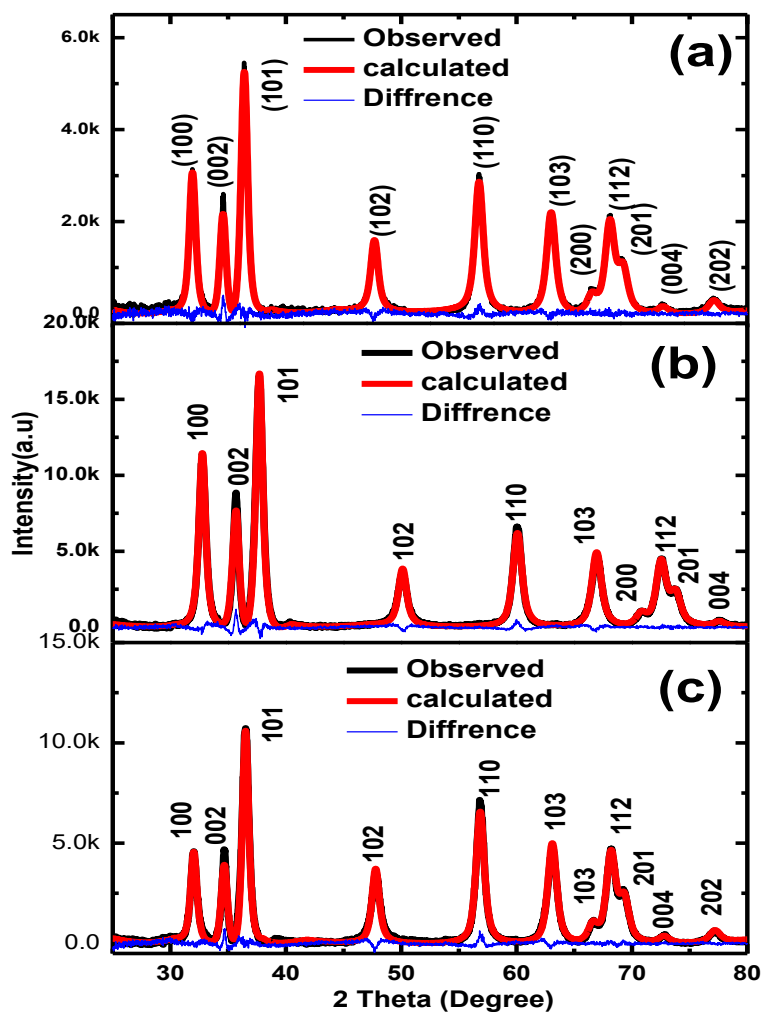


Figure 3.1: XRD pattern of ZnO nanoparticles (a), sample-D (b), and sample-E (c)

To find good refinement results, some parameters such as zero error and absorption correction factors were taken under consideration. The calculated goodness of fit (GOF) from Rietveld refinement was close to 1 after appropriate corrections employing spherical harmonics. An order of 5 was used for Chebychev background correction. All XRD plots confirm the crystallographic structure of ZnO nanoparticles which indicates that ZnO nanoparticles of all samples are crystallized as *P63mc* (hexagonal close-packed crystal structure). The lattice parameters *a* and *c* are determined for ZnO nanoparticles and nanoconjugates of ZnO-thymine and ZnO-cytosine. There is no apparent change in the lattice parameters *a*, *c*, and *c/a* ratio, given in Table 3.1, for ZnO nanoparticles and the nanoconjugates. From the data analysis, there is no significant change in the structural properties of ZnO nanoparticles after interaction with thymine and cytosine biomolecules. Results also indicate that the nano-bio interaction has taken place on the surface of ZnO nanoparticles which has been proved by the Raman spectroscopy, PL, and XPS.

Table 3.1: Lattice parameters, *c/a* ratio of sample-A, D, and E

Sample ID	Lattice parameter <i>a</i> (\AA)	Lattice Parameter <i>c</i> (\AA)	<i>c/a</i>
A	3.25	5.21	1.602
D	3.24	5.19	1.602
E	3.23	5.18	1.602

The vibrational modes of ZnO nanoparticles are easily described by the Raman spectroscopy. The molecular vibrational modes of ZnO nanoparticles have been studied

using micro Raman spectroscopy. Figure 3.2 shows the Raman spectra of pure ZnO nanoparticles consist of three prominent vibrational modes at around 336cm^{-1} , 438cm^{-1} , and 580cm^{-1} along with some other weak signals at around 984cm^{-1} , 1046cm^{-1} , and 1094cm^{-1} . The Raman peaks at 336cm^{-1} , 438cm^{-1} and 580cm^{-1} are identified as ($E_{2H}-E_{2L}$), E_2 (High), and E_1 (LO) modes, and the peaks at around 984cm^{-1} and 1094cm^{-1} are assigned for $A_1(\text{LO})+E_2\text{High}$, and (2LO) modes respectively¹⁷⁻¹⁸. Another Raman peak at 1046cm^{-1} is basically originated for C-O asymmetric mode of carboxylate defect group, and this peak is affected by the surface area and the particle size of materials¹⁹.

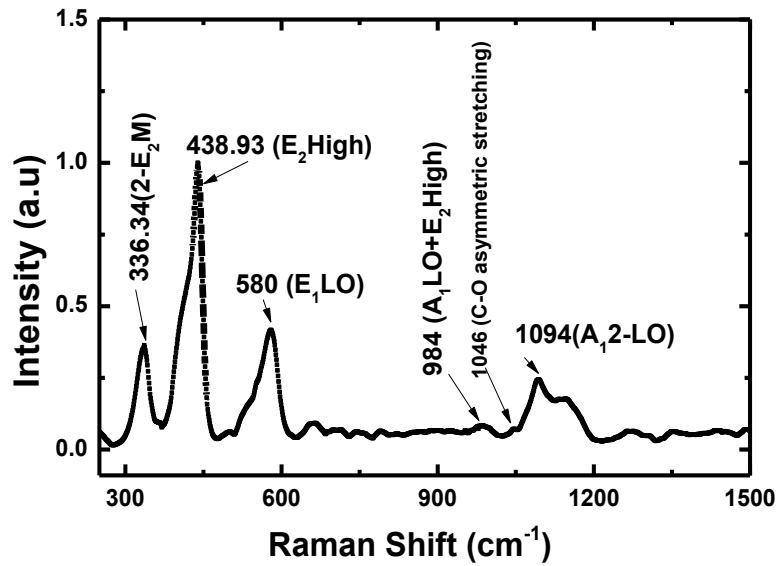


Figure 3.2: Raman spectra of ZnO nanoparticle

The molecular vibration at 336cm^{-1} appears for the low frequency Raman bands associated for the difference between $E_2(\text{High})$ and $E_2(\text{Low})$ modes¹⁸. The most prominent mode centered at 438cm^{-1} is originated to the oxygen vibration in hexagonal crystalline structure of ZnO nanoparticles along the X-Y plane and this peak becomes

wider due to incorporation with foreign molecules on the ZnO surface layer¹⁹. The sharpest E₂ High mode indicates the more homogenous distribution of grain sizes and the dimension of ZnO nanoparticles⁴. For sample-A, 438 cm⁻¹ peak appears as the most intensely that revealed that all samples are more homogeneously distributed with significant particle size. The second sharpest peak at 580 cm⁻¹ is assigned for the oxygen deficiency on the surface of ZnO nanoparticles which is namely E₁ longitudinal optical (LO)²⁰. This Raman vibrational mode indicates the defect or the impurity on the surface layer which originated for the oxygen (O) vacancy and the zinc (Zn) interstitials on the ZnO nanostructure⁴. The peak at 984 cm⁻¹ is interpreted as A₁(LO)+E₂High mode which is associated for the vibration of two phonon combination and the secondary A₁ longitudinal optical mode (2LO) at 1094 cm⁻¹ is created for the molecular vibration along the Z-axis of ZnO nanoparticles⁴. The C-O asymmetric mode of carboxylate defect group is also associated at 1046 cm⁻¹ which is changed by the changing of surface area and the particles size of nanostructure¹⁹. The molecular structures of thymine and cytosine biomolecules have been shown in Figure 3.3 and Figure 3.4 respectively.

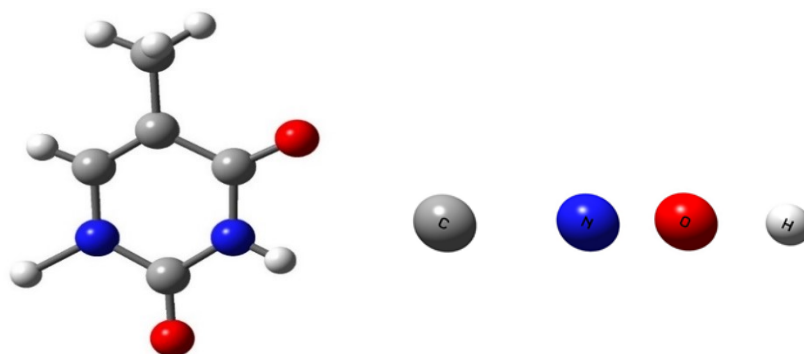


Figure 3.3: Molecular structure of thymine

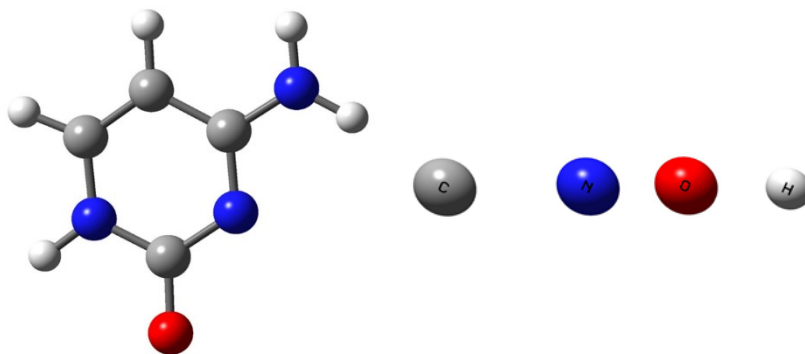


Figure 3.4: Molecular structure of cytosine

Figure 3.5 indicates the Raman spectra of thymine powder (a), and hydrolyzed thymine (b). All spectra were taken in a same time by using 532 green laser sources.

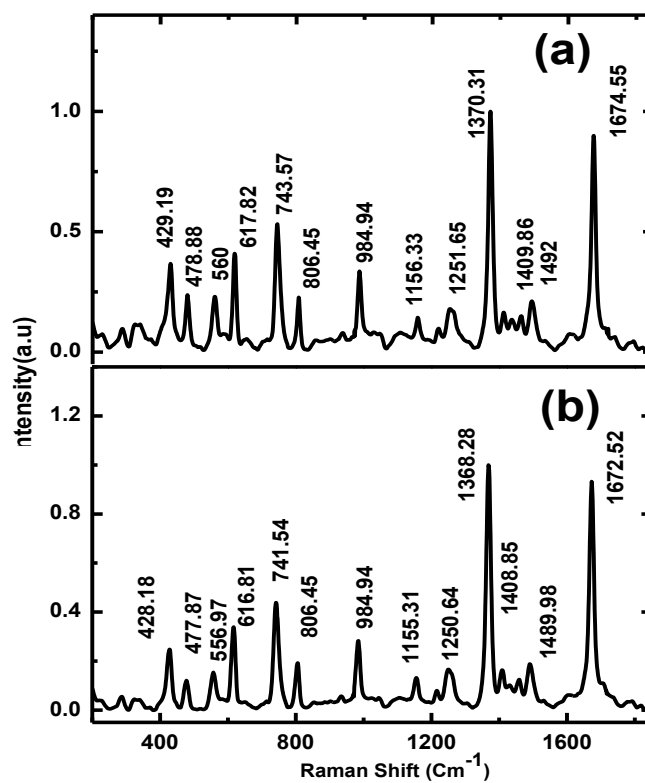


Figure 3.5: Raman spectra of thymine powder (a), and hydrolyzed thymine (b)

The Raman spectrum of pure thymine consists of several peaks due to the ring breath, bend, stretch, wag of C=O, C-H and N-H molecular bonds^{11,21-22}. Dissolution of thymine involves cation affinity and hydrogen bonds with water molecules¹¹. After interaction with water molecule, significant Raman shift due to the cation affinity of thymine can play an active role in hydrogen bond formation. The cation affinity of thymine biomolecule may increase with the incorporation of Zn²⁺ ion of ZnO nanoparticles because according to the cation reactivity series, Zn²⁺ is more active than cation H⁺¹¹. In pure thymine (Figure 3.5(a)), the Raman band at 560cm⁻¹ and 1370 cm⁻¹ are assigned for the bend of C2-O7, C4-O8, and C5-CH3 bonds and N3-H, C6-H bonds, respectively¹¹. Peaks at 1490 cm⁻¹, 1672 cm⁻¹ are associated for the bend of N1-H, C6-H and stretch of C4-C5, C4=O8, bend of N1-H, C6-H, respectively¹¹. Figure 3.6 display the comparison Raman spectra of thymine powder and hydrolyzed thymine (a), and Raman spectra of thymine powder, hydrolysis thymine, and sample-D (b). It is clearly shown that, on hydrolyzed thymine and on ZnO-thymine nanoconjugate, thymine biomolecule indicates the cation affinity of C2=O7, C4=O8 sites. Thus, the 560cm⁻¹ mode is shifted to 557cm⁻¹ position for a bend of C2=O7, C4=O8 bonds. Due to the stretch of C4=O8 bond, C4-C5 bond and a bend N1-H, C6-H molecular bonds 1674 cm⁻¹ mode is also shifted to 1674 cm⁻¹ to Sample-C and 1669 cm⁻¹ to Sample-D. Another Raman vibrational mode at 1370 cm⁻¹ which is created for the bending of N3-H, C6-H modes on pure thymine is also shifted to 1368 cm⁻¹ for hydrolysis thymine and 1357 cm⁻¹ for ZnO-thymine nanoconjugate. This significant peak position shift can be assigned for the more cation affinity of C2=O7, C4=O8 sites after incorporation of ZnO nanoparticles. Thus, Zn²⁺ may create a bond with C2=O7 or C4=O8 sites of thymine. Assignments of the vibrational

mode of thymine, hydrolysis thymine and ZnO-thymine nanoconjugate are given in Table 3.2.

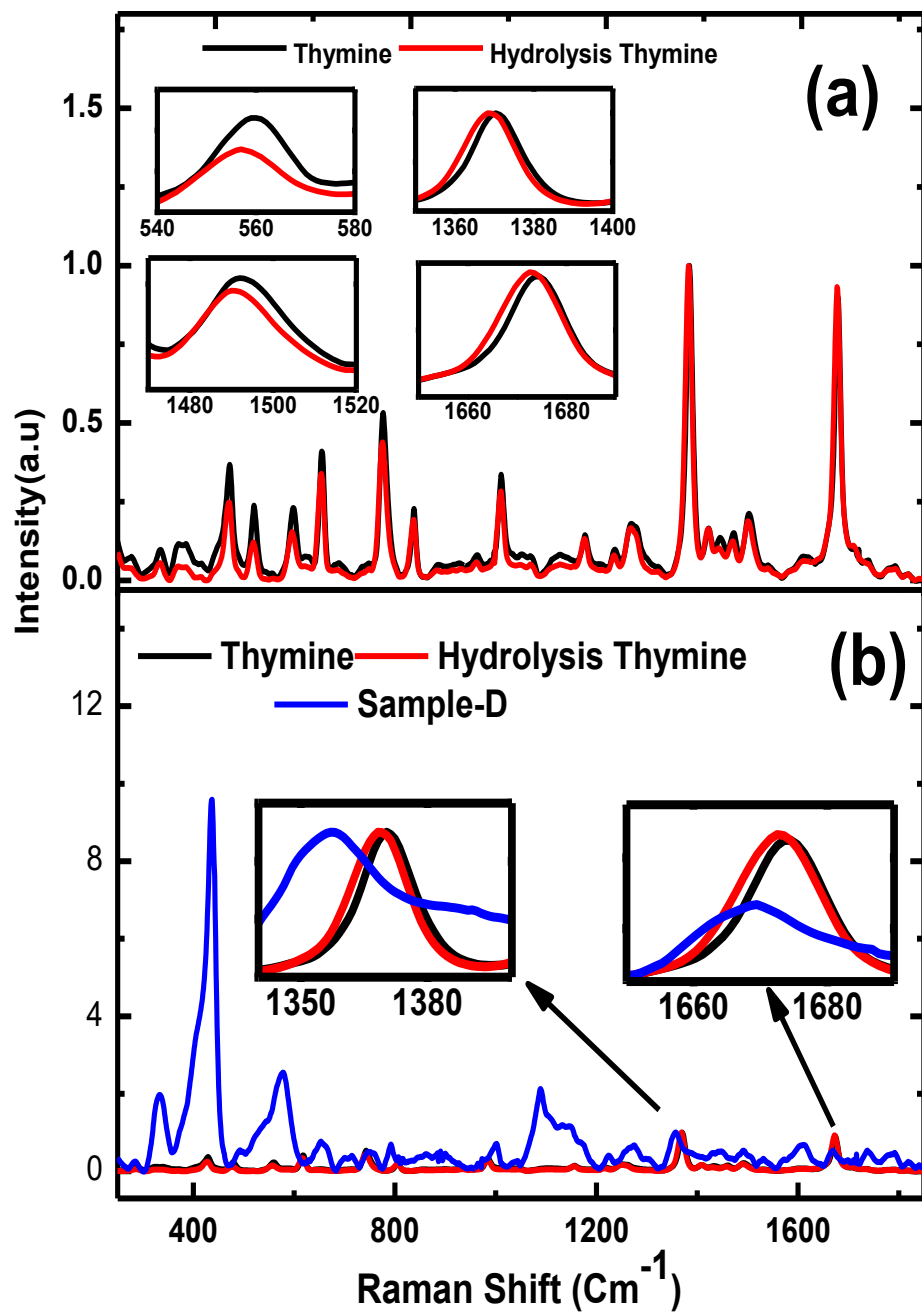


Figure 3.6: Comparison Raman spectra of thymine powder and hydrolyzed thymine (a), and Raman spectra of thymine powder, hydrolysis thymine, and sample-D (b)

Table 3.2: Assignments of the vibrational mode of thymine, hydrolysis thymine and ZnO-thymine nanoconjugate

Thymine (cm^{-1})	(Sample-C) (cm^{-1})	(Sample-E) (cm^{-1})	Description
429	428		A bend C2-O, C4-O
479	478		Squeeze ring
560	557		A bend C2-O, C4-O, C5-CH3
618	617		Wag N3-H
743	741		Ring breath
806	806		Stretch C5-CH3
1156	1155		Stretch N3-C4
1251	1250		Stretch N1-C6, C5-CH3
1370	1368	1357	A bend N3-H, C6-H
1492	1490		A bend N1-H, C6-H
1674	1672	1669	Stretch C4-C5, C4=O, A bend N1-H, C6-H

Figure 3.7(a,b) show the Raman spectra of cytosine powder and hydrolysis cytosine. Cytosine in water molecules can create the hydrogen bond for the cation with C2=O2 which can attract the proton (H^+) and N-H site can create a bond with hydroxyl group (OH^-) of water molecule¹². Similarly, hydrolysis ZnO can be ionized as Zn^{2+} and O^{2-} . It may assume that oxygen atom can be attached with N8-H9 site of amino group or N1-H1 site of cytosine ring. On the other hand, Zn^{2+} cation can be attached by N3 atom or C2-O2 site due to the cation affinity of DNA base (cytosine). The sharpest peaks of pure

cytosine (Figure 3.7 (a)) at around 790 cm^{-1} is assigned for the out-of-plane deformation of $\text{C}=\text{O}$ along with ring vibration and at around 1276 cm^{-1} is for in-plane deformation of $\text{C}6\text{-H}$ bond and stretching of $\text{C}2\text{-N}3$ bond²². There is another significant change for stretching of $\text{C}2\text{-N}3$ bond and for in-plane deformation of $\text{C}6\text{-H}$ bond. The molecular vibration at 1462 cm^{-1} for in-plane deformation of $\text{N}1\text{-H}$ and stretching of $\text{N}1\text{-C}2$ and $\text{N}3\text{-C}4$ sites has been shifted to 1450 cm after incorporation of water molecules²².

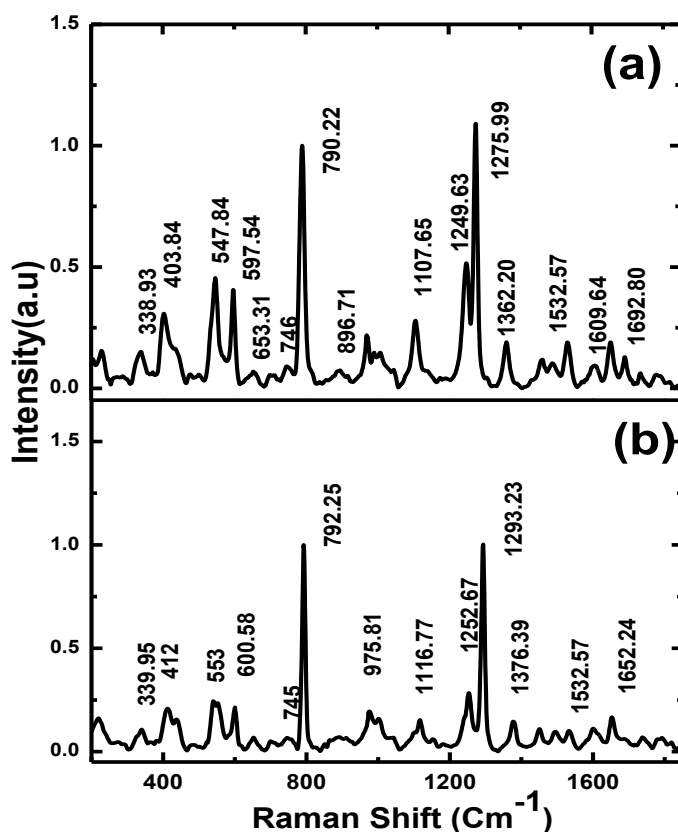


Figure 3.7: Raman spectra of cytosine powder (a), and hydrolysis cytosine (b)

Figure 3.8 indicate the comparison of Raman spectra of cytosine powder and hydrolyzed cytosine (a), comparative Raman spectra of sample-A, B, E (b), and comparative Raman

spectra of cytosine powder, sample-A, B, and E (c). Table 3.3 indicates the assignments of the vibrational modes of cytosine, hydrolyzed cytosine, and ZnO-cytosine nanoconjugates.

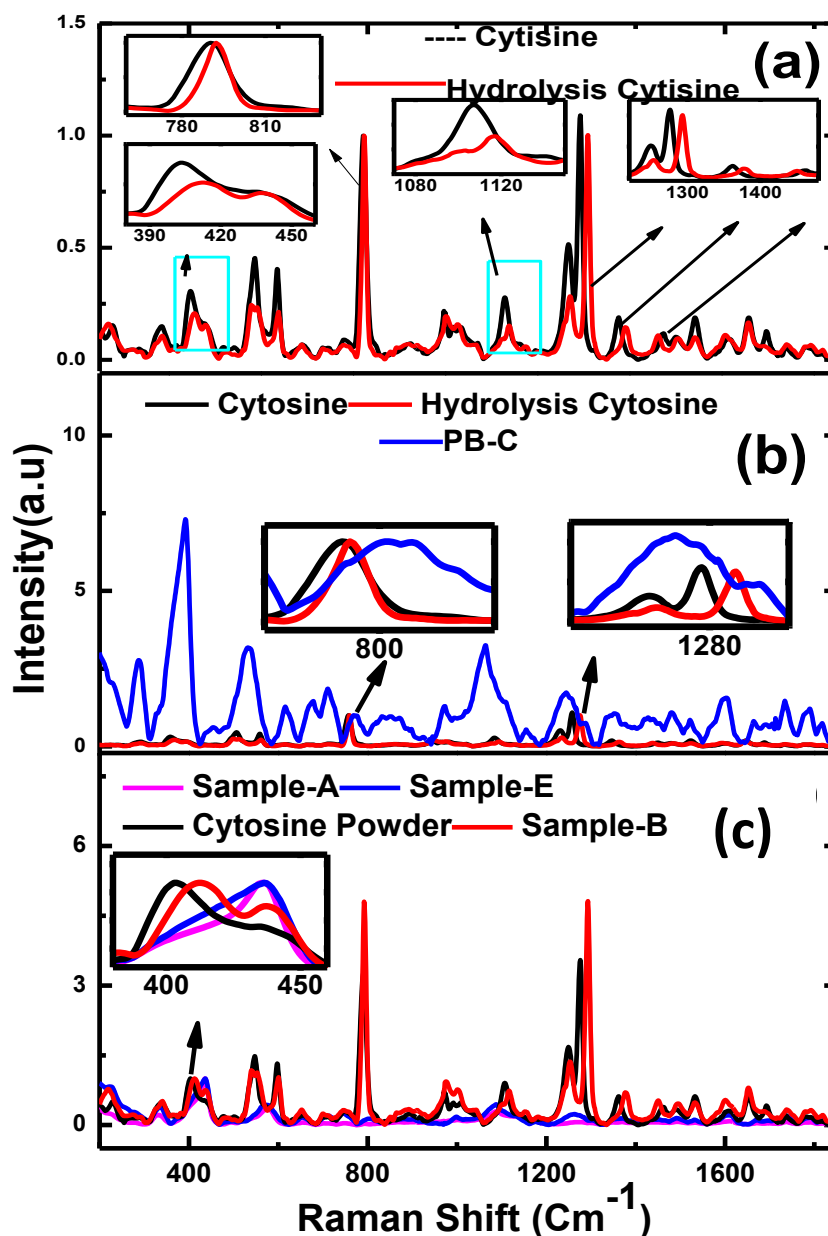


Figure 3.8: Comparison of Raman spectra of cytosine powder and hydrolyzed cytosine (a), comparative Raman spectra of sample-A, B, E (b), comparative Raman spectra of cytosine powder, sample-A, B, and E (c)

Table 3.3: Assignments of the vibrational modes of cytosine, hydrolyzed cytosine, and ZnO-cytosine nanoconjugates

Cytosine (cm^{-1})	(Sample-B) (cm^{-1})	Description
339	340	Ring out-of plane deformation, wagging NH ₂
404	412	Ring vibration
548	553	Ring in-plane deformation, torsion of NH ₂
597	600	In-plane deformation of ring and C=O
653	652	Out-of-plane deformation N1-H
790	792	Out of plane deformation C=O and ring vibration
1107	1116	Rocking of NH ₂
1249	1252	Ring Stretching, in-plane deformation C5-H and N1-H
1276	1293	Stretching C2-N3, in-plane deformation C6-H
1362	1376	Stretching C4-N8, in-plane deformation of C5-H and C6-H
1462	1450	In-plane deformation N1-H, Stretching of N1-C2 and N3-C4

Figures 3.9(a,b) show the room temperature PL spectra of ZnO Bulk, and ZnO nanoparticles respectively. An excitation peak near the band gap of ZnO nanopowder and a broad emission for the surface defect of the nanostructure are appeared on the PL spectra. The PL data was fitted using several Gaussians using Origin.pro 8.5.1 software.

The PL spectra of ZnO nanoparticles at the room temperature gives an ultraviolet spectra emission at around 385 nm due to band-band transition. The surface defects are originated due to oxygen vacancies, Zn_i , O_i , Zn vacancies on the different states of the ZnO surface layer which is called green-yellow-orange emission^{3,17}. These defects depend on the particle sizes, fabrication process, and the impurity on the nanoparticles²³. Blue emission also appears at around 470 nm range for the Zinc vacancies along with interstitial oxygen on the surface of ZnO nanostructures.

The green emission at around 520nm is originated due to the recombination of photo generated hole with the electron in the single ionized oxygen vacancies and the yellow emission is responsible for the delocalized electrons which are very close to conduction band of the ZnO surface layer with a deep trap hole in the O_i center^{7,24}.

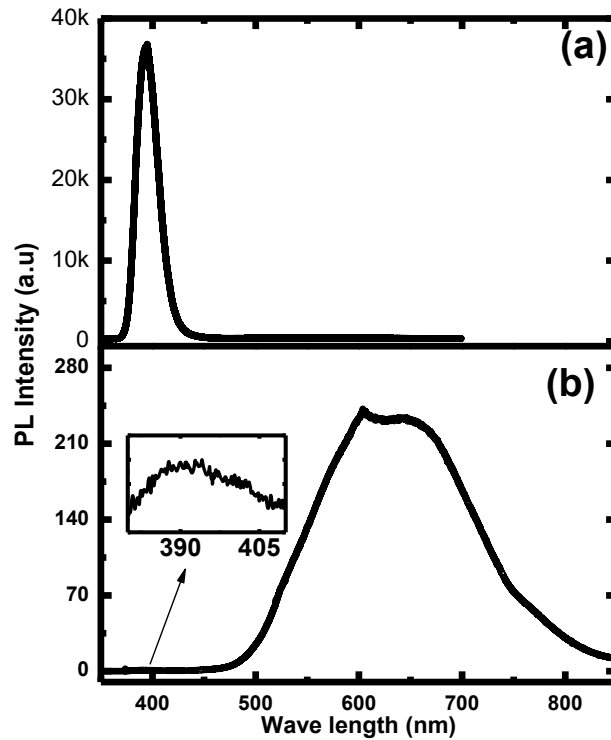


Figure 3.9: Room Temperature PL spectra of ZnO Bulk (a), and ZnO nanoparticle (b)

On the surface layer of ZnO nanostructure, there are three different charge states of oxygen vacancy namely the neutral oxygen vacancies, single ionized, and double ionized oxygen vacancies. Due to thermodynamically instability of single ionized oxygen vacancies, there will be only neutral and double ionized oxygen vacancies depending on the position of fermi level on the surface layer³. Having the very small surface volume of ZnO nanostructures, the quasi fermi level of electrons can cross the certain level by the very low excitation energy so that oxygen vacancies will have very lowest energy compare with others defect reasons³. So, it is more generalized now that the defect on the surface layer is mostly responsible for the particle sizes and the surface to volume ratio which increase the density of the oxygen vacancies of ZnO nanostructures²⁵. Figure 3.10 indicates the PL spectra of ZnO nanoparticles and nano-bio conjugates.

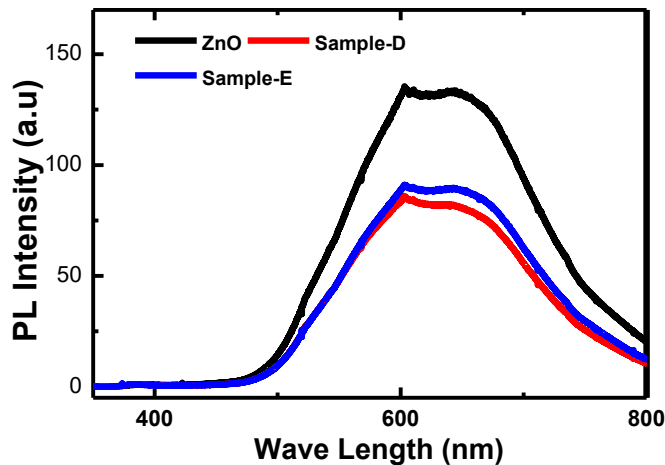


Figure 3.10: PL spectra of ZnO (Black), sample-D (Red), and sample-E (Blue)

The PL data of ZnO-thymine (sample-D) and ZnO-cytosine (sample-E) nano-bio conjugates revealed that the defect is decreased with the incorporation of DNA bases on

the ZnO surface layer. Thymine and cytosine both have oxygen atoms on their molecular structure, and oxygen can be absorbed by the surface layer of the ZnO nanostructure. By absorbing oxygen atoms on the ZnO surface layer, oxygen vacancies decrease that cause to decrease green-yellow defect emission from the ZnO nanostructures. Table 3.4 shows the decreasing of defect peak area of ZnO-thymine and ZnO-cytosine conjugates compare to ZnO nanoparticles. From Table 3.4, it is clearly shown that the surface defect is decreased with incorporation of cytosine and thymine on ZnO nanoparticles. The surface defects are decreased due to binding ZnO with thymine as well as cytosine.

Table 3.4: PL peak positions (nm) and the defect area (nm²)

Sample ID	Band peak area (nm ²)	Defect peak area (nm ²)
ZnO	66.66	24968.89
Sample-D	47.69	15489.80
Sample-E	42.80	16729.27

Figure 3.11 show the SEM images of the nanoconjugates. TEM images have been shown in Figure 3.12. The average particle size of ZnO nanoparticles is 20-30 nm. Table 3.5 confirms the different concentrations (atom%) of Zn and O for ZnO-thytosine and ZnO-thymine nanoconjugates. EDX data revealed that O concentration (atom %) has been increased for both of nanoconjugates compare with the ZnO nanoparticles. Figures 3.13 show the XPS data of Zn 2p core shell level on ZnO, ZnO-cytosine nano-conjugate (a), and ZnO, ZnO-thymine conjugate (b). The intensity of Zn 2p core shell peak is decreased for the ZnO-DNA bases nanoconjuagtes compare with the ZnO nanoparticles which is

expected. The lower intensity indicates the thymine and cytosine coating on the surface layer of ZnO nanoparticles.

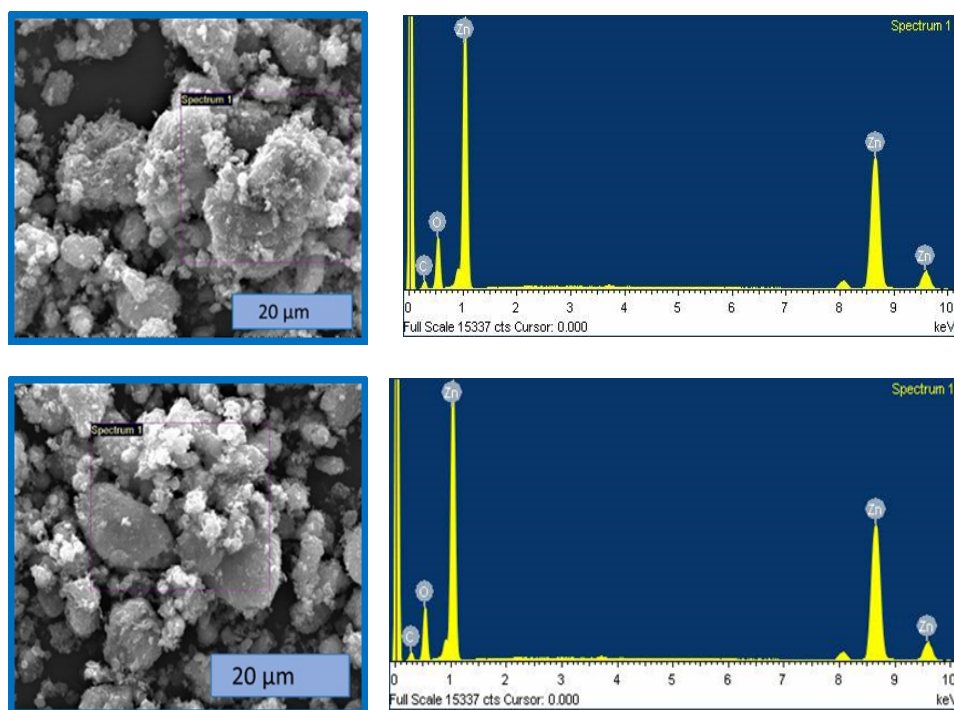


Figure 3.11: SEM images and EDX data of sample PB-D (Top), sample PB-E (Bottom)

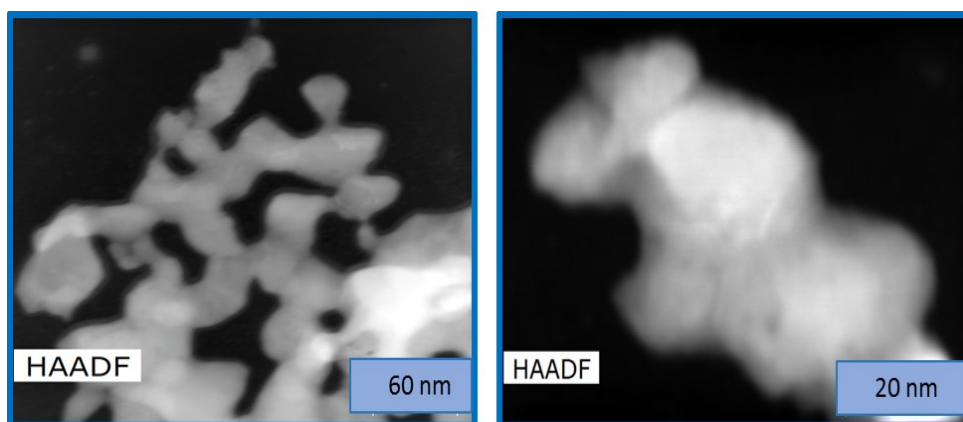


Figure 3.12: TEM images of ZnO nanoparticle

Table 3.5: Zn and O concentrations (atom %) on ZnO and nanoconjugates

Sample ID	Zn concn(Atom %)	O concn (Atom %)	C concn(Atom %)
ZnO	62.02	37.98	00.00
PB-E	35.93	24.02	40.04
PB-D	48.71	27.52	23.78

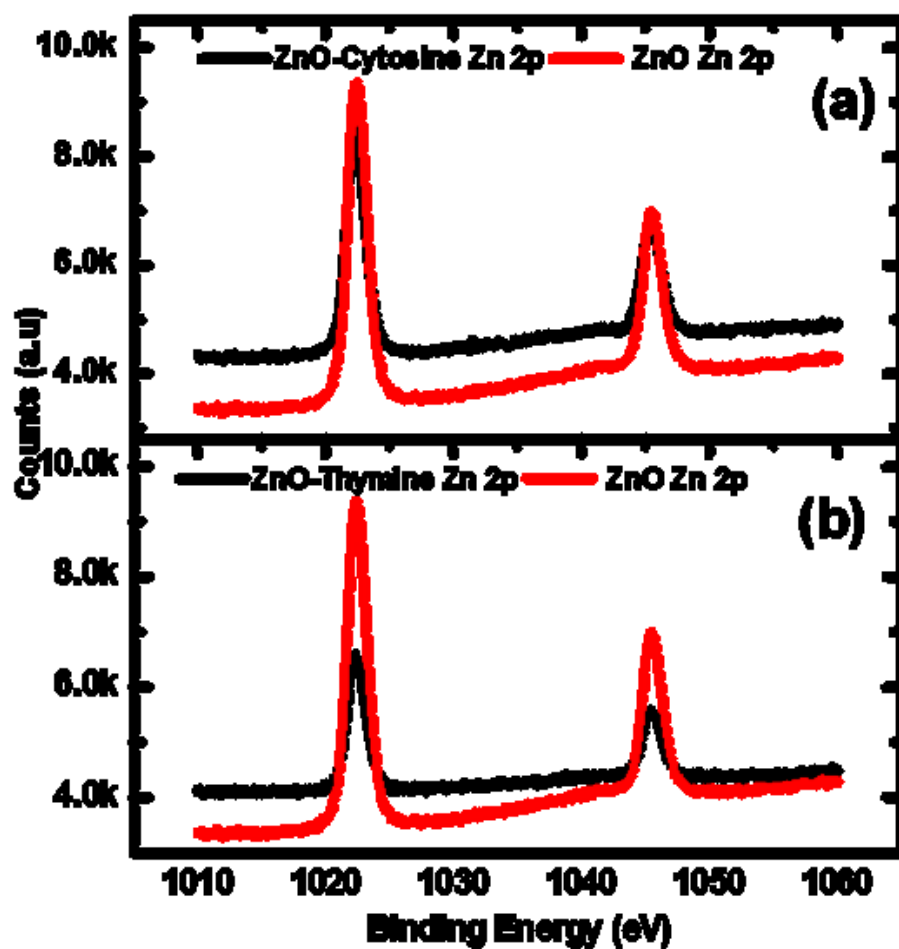


Figure 3.13: XPS data of Zn 2p core shell level on ZnO, ZnO-cytosine nano-conjugate (a), ZnO, ZnO-thymine conjugate (b)

Figure 3.14 indicates the X-ray photoelectron spectra of N 2p core shell electron of cytosine, ZnO-cytosine nano-bio conjugate (a) and thymine, ZnO-thymine nano-bio conjugate (b). X-ray photoelectron spectra confirm the presence of N atom on the cytosine and thymine both nitrogenous bases. The N 2p peak is more visible on ZnO-cytosine and thymine both nitrogenous bases. The N 2p peak is more visible on ZnO-cytosine and ZnO-Thymine nano-bio conjugates.

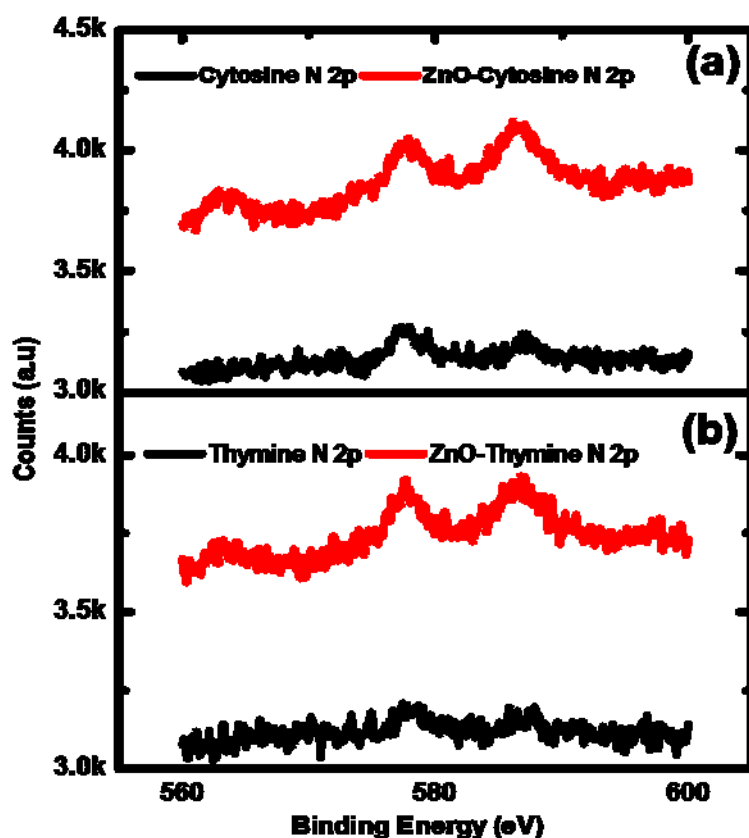


Figure 3.14: X-ray photoelectron spectra of N 2p core shell electron of cytosine, ZnO-cytosine nano-bio conjugate (a) and thymine, ZnO-thymine nano-bio conjugate (b)

Figure 3.15 (a,b) exhibit the XPS data O 1s core shell for ZnO, the ZnO –thymine, and ZnO-cytosine nano-bio conjugates. Figure 3.15 (a) reveals that The peaks position of

ZnO-Thymine and ZnO-Cytosine are in between the DNA bases O 1s and ZnO O 1s peak which suggest that there have some interaction with ZnO and DNA bases on the nano-bio conjugated materials.

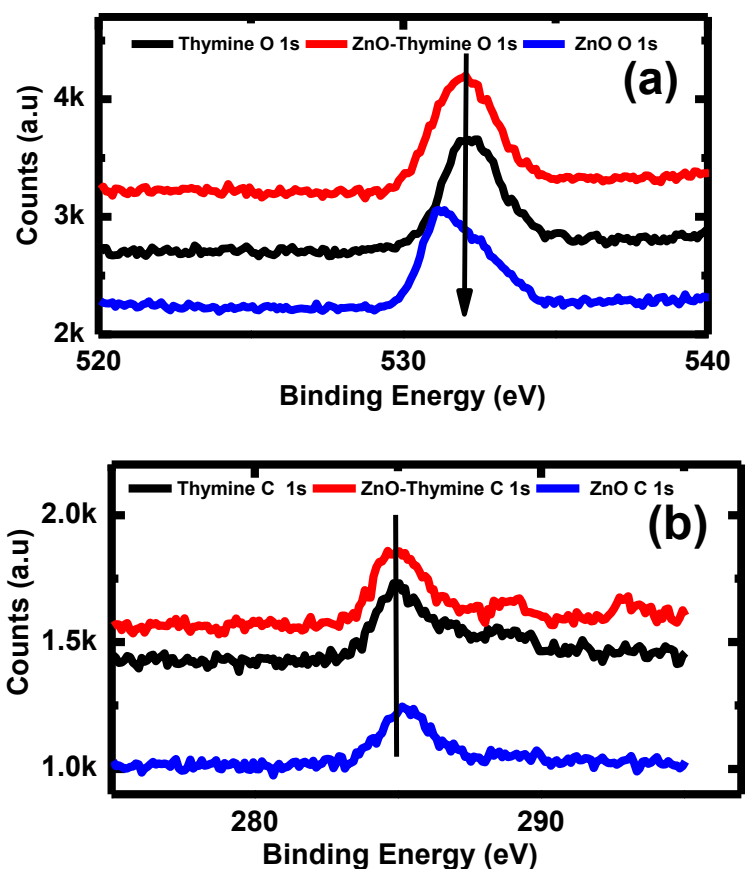


Figure 3.15: XPS data of O 1s core shell (a), and C 1s core shell (b) of ZnO, thymine, and ZnO-thymine nano-bio conjugates

Conclusions

In this work, the cation affinity has been observed in both thymine and cytosine after interacting with ZnO nanoparticles. Some of the molecular vibrations of cytosine and thymine biomolecules are changed with the interaction of ZnO nanostructure. The

Raman wave number for the molecular vibration of C2=O7, C4=O8 sites for thymine biomolecule have been shifted due to cation affinity after incorporation of water molecules as well as ZnO nanoparticles. Similarly, wave number of C=O and N-H vibrations are shifted for the cytosine by the attraction of cations (Zn^{2+} , H^+). So, it can be assumed that ZnO nanoparticles bind with the DNA bases (Thymine, Cytosine) and the nanoconjugates can be used for targeted drug delivery or nanomedicine applications. PL as well as XPS data also support the Raman data.

References

1. Xu, C., Yang, C., Gu, B. & Fang, S. Nanostructured ZnO for biosensing applications. *Chin. Sci. Bull.* **58**, 2563–2566 (2013).
2. Gurwitz, R., Cohen, R. & Shalish, I. Interaction of light with the ZnO surface: Photon induced oxygen ‘breathing,’ oxygen vacancies, persistent photoconductivity, and persistent photovoltage. *J. Appl. Phys.* **115**, 33701 (2014).
3. Gong, Y., Andelman, T., Neumark, G. F., O’Brien, S. & Kuskovsky, I. L. Origin of defect-related green emission from ZnO nanoparticles: Effect of surface modification. *Nanoscale Res. Lett.* **2**, 297–302 (2007).
4. Wong, K. W. J. *et al.* Interaction of hydrogen with ZnO nanopowders—evidence of hydroxyl group formation. *Nanotechnology* **23**, 15705 (2012).
5. Srivastava, R. Investigation on Temperature Sensing of Nanostructured Zinc Oxide Synthesized via Oxalate Route. *J. Sens. Technol.* **2**, 8–12 (2012).
6. Demangeot, F. *et al.* Experimental study of LO phonons and excitons in ZnO nanoparticles produced by room-temperature organometallic synthesis. *Appl. Phys. Lett.* **88**, 71921 (2006).
7. Liu, J., Motta, N. & Lee, S. Ultraviolet photodetection of flexible ZnO nanowire sheets in polydimethylsiloxane polymer. *Beilstein J. Nanotechnol.* **3**, 353–359 (2012).
8. Alvi, N. ul H., Hussain, S., Jensen, J., Nur, O. & Willander, M. Influence of helium-ion bombardment on the optical properties of ZnO nanorods/p-GaN light-emitting diodes. *Nanoscale Res. Lett.* **6**, 628 (2011).

9. Kuriakose, S., Satpati, B. & Mohapatra, S. Enhanced photocatalytic activity of Co doped ZnO nanodisks and nanorods prepared by a facile wet chemical method. *Phys. Chem. Chem. Phys.* **16**, 12741 (2014).
10. Zhang, Y., Nayak, T. R., Hong, H. & Cai, W. Biomedical Applications of Zinc Oxide Nanomaterials. *Curr. Mol. Med.* **13**, 1633–1645 (2013).
11. Shang, Z.-G. *et al.* A study of DFT and surface enhanced Raman scattering in silver colloids for thymine. *J. Mol. Struct.* **826**, 64–67 (2007).
12. Chandra, A. ., Nguyen, M. . & Zeegers-Huyskens, T. Theoretical study of the protonation and deprotonation of cytosine. Implications for the interaction of cytosine with water. *J. Mol. Struct.* **519**, 1–11 (2000).
13. Sánchez-Cortés, S. & García-Ramos, J. V. Influence of coverage in the surface-enhanced Raman scattering of cytosine and its methyl derivatives on metal colloids: Chloride and pH effects. *Surf. Sci.* **473**, 133–142 (2001).
14. Ahmadi, M. S. & Fattahi, A. On the binding of Mg^{2+} , Ca^{2+} , Zn^{2+} and Cu^{+} metal cations to 2' -deoxyguanosine: Changes on sugar puckering and strength of the -glycosidic bond. *Sci. Iran.* **18**, 1343–1352 (2011).
15. Anwender, E. H. S., Probst, M. M. & Rode, B. M. The influence of Li^{+} , Na^{+} , Mg^{2+} , Ca^{2+} , and Zn^{2+} ions on the hydrogen bonds of the Watson-Crick base pairs. *Biopolymers* **29**, 757–769 (1990).
16. Gresh, N. & Šponer, J. Complexes of Pentahydrated Zn^{2+} with Guanine, Adenine, and the Guanine–Cytosine and Adenine–Thymine Base Pairs. Structures and Energies Characterized by Polarizable Molecular Mechanics and ab Initio Calculations. *J. Phys. Chem. B* **103**, 11415–11427 (1999).
17. Camarda, P. *et al.* Luminescence mechanisms of defective ZnO nanoparticles. *Phys Chem Chem Phys* **18**, 16237–16244 (2016).
18. Jan, T., Iqbal, J., Ismail, M. & Mahmood, A. Synthesis of highly efficient antibacterial agent Ag doped ZnO nanorods: Structural, Raman and optical properties. *J. Appl. Phys.* **115**, 154308 (2014).
19. Xiong, G., Pal, U. & Serrano, J. G. Correlations among size, defects, and photoluminescence in ZnO nanoparticles. *J. Appl. Phys.* **101**, 24317 (2007).
20. Rajalakshmi, M., Arora, A. K., Bendre, B. S. & Mahamuni, S. Optical phonon confinement in zinc oxide nanoparticles. *J. Appl. Phys.* **87**, 2445–2448 (2000).
21. Singh, J. S. FTIR and Raman spectra and fundamental frequencies of biomolecule: 5-Methyluracil (thymine). *J. Mol. Struct.* **876**, 127–133 (2008).

22. Aroca, R. & Bujalski, R. Surface enhanced vibrational spectra of thymine. *Vib. Spectrosc.* **19**, 11–21 (1999).
23. Yadav, H. K., Sreenivas, K., Gupta, V., Singh, S. P. & Katiyar, R. S. Effect of surface defects on the visible emission from ZnO nanoparticles. *J. Mater. Res.* **22**, 2404–2409 (2007).
24. Panda, S. K. & Jacob, C. Surface enhanced Raman scattering and photoluminescence properties of catalytic grown ZnO nanostructures. *Appl. Phys. A* **96**, 805–811 (2009).
25. Naeem, M., Qaseem, S., Gul, I. H. & Maqsood, A. Study of active surface defects in Ti doped ZnO nanoparticles. *J. Appl. Phys.* **107**, 124303 (2010).

CHAPTER 4: CONCLUSIONS

In this study, I have fabricated three types of nano-bio conjugates and characterized those conjugates using various spectroscopic techniques to better understand nano-bio interfaces. Raman spectroscopy, XPS, and PL spectroscopy data reveal that the surface of ZnO nanostructures is uniformly coated with glucose biomolecules by capturing free electrons from the surface layer of ZnO nanostructures. Due to having the single and double ionized oxygen vacancies on the surface area of ZnO nanostructures, oxygen atoms from glucose are absorbed by capturing free electrons. Consequently, the green emission, originated by the oxygen vacancies on ZnO nanostructures, has been reduced. High glucose concentrations notably quench the defect area of nanostructures and decrease the surface to volume ratio. The changes of some Raman vibrational modes of ZnO-glucose nano-bio conjugates also divulge that incorporation of glucose biomolecules on ZnO nanoparticles effects some of the vibrational modes of ZnO nanoparticles, which is also useful to identify the quantification of glucose on ZnO nanoparticles. Increasing glucose concentration widens E_2 High and increases the intensity of A_12+ LO modes. The XPS and EDX data also indicate uniform coating of glucose on the surface of ZnO nanoparticles.

Some of the Raman vibrational modes of DNA bases are shifted due to having the cation affinity on those bases. Thymine shows the cation affinity on C2=O7, C4=O8 sites and cytosine shows cation affinity on C2=O2 site. Water molecules give H^+ and ZnO nanomaterials give Zn^{2+} cation in the solution. Both cations are attracted by the cytosine and thymine while they formed as nano-bio composite. Therefore, it can be confirmed

that due to cation affinity of DNA, transition metal cation (Zn^{2+}) can be nicely bonded with cytosine and thymine nitrogenous bases. XPS data also support this mechanism. The PL data reveal that surface defect of ZnO nanoparticles can be minimized with incorporation of DNA bases. The study of nano-bio conjugates will provide remarkable biological applications like targeted drug delivery, diabetes sensor, and bioimaging.

CHAPTER 5: REFERENCES

1. Zhang, Y., Nayak, T. R., Hong, H. & Cai, W. Biomedical Applications of Zinc Oxide Nanomaterials. *Curr. Mol. Med.* **13**, 1633–1645 (2013).
2. Naeem, M., Qaseem, S., Gul, I. H. & Maqsood, A. Study of active surface defects in Ti doped ZnO nanoparticles. *J. Appl. Phys.* **107**, 124303 (2010).
3. Gong, Y., Andelman, T., Neumark, G. F., O'Brien, S. & Kuskovsky, I. L. Origin of defect-related green emission from ZnO nanoparticles: Effect of surface modification. *Nanoscale Res. Lett.* **2**, 297–302 (2007).
4. Wong, K. W. J. *et al.* Interaction of hydrogen with ZnO nanopowders—evidence of hydroxyl group formation. *Nanotechnology* **23**, 15705 (2012).
5. Srivastava, R. Investigation on Temperature Sensing of Nanostructured Zinc Oxide Synthesized via Oxalate Route. *J. Sens. Technol.* **2**, 8–12 (2012).
6. Demangeot, F. *et al.* Experimental study of LO phonons and excitons in ZnO nanoparticles produced by room-temperature organometallic synthesis. *Appl. Phys. Lett.* **88**, 71921 (2006).
7. Liu, J., Motta, N. & Lee, S. Ultraviolet photodetection of flexible ZnO nanowire sheets in polydimethylsiloxane polymer. *Beilstein J. Nanotechnol.* **3**, 353–359 (2012).
8. Alvi, N. ul H., Hussain, S., Jensen, J., Nur, O. & Willander, M. Influence of helium-ion bombardment on the optical properties of ZnO nanorods/p-GaN light-emitting diodes. *Nanoscale Res. Lett.* **6**, 628 (2011).
9. Kuriakose, S., Satpati, B. & Mohapatra, S. Enhanced photocatalytic activity of Co doped ZnO nanodisks and nanorods prepared by a facile wet chemical method. *Phys. Chem. Chem. Phys.* **16**, 12741 (2014).
10. Rahman, M. M., Ahammad, A. J. S., Jin, J.-H., Ahn, S. J. & Lee, J.-J. A Comprehensive Review of Glucose Biosensors Based on Nanostructured Metal-Oxides. *Sensors* **10**, 4855–4886 (2010).
11. Zhuang, Z. *et al.* An improved sensitivity non-enzymatic glucose sensor based on a CuO nanowire modified Cu electrode. *The Analyst* **133**, 126–132 (2008).
12. Yu, R., Pan, C., Chen, J., Zhu, G. & Wang, Z. L. Enhanced Performance of a ZnO Nanowire-Based Self-Powered Glucose Sensor by Piezotronic Effect. *Adv. Funct. Mater.* **23**, 5868–5874 (2013).

13. Lyandres, O. *et al.* Progress Toward an In Vivo Surface-Enhanced Raman Spectroscopy Glucose Sensor. *Diabetes Technol. Ther.* **10**, 257–265 (2008).
14. Bhaumik, A., Shearin, A. M., DeLong, R., Wanekaya, A. & Ghosh, K. Probing the Interaction at the Nano–Bio Interface Using Raman Spectroscopy: ZnO Nanoparticles and Adenosine Triphosphate Biomolecules. *J. Phys. Chem. C* **118**, 18631–18639 (2014).
15. Xu, C., Yang, C., Gu, B. & Fang, S. Nanostructured ZnO for biosensing applications. *Chin. Sci. Bull.* **58**, 2563–2566 (2013).